Molecular Biology of the Cell
Vol. 17, 5115–5130, December 2006

# Myristoylated, Alanine-rich C-Kinase Substrate Phosphorylation Regulates Growth Cone Adhesion and Pathfinding

**Jesse C. Gatlin,* Adriana Estrada-Bernal,† Staci D. Sanford,† and Karl H. Pfenninger**

Departments of Pediatrics and of Cell and Developmental Biology, University of Colorado School of Medicine, and University of Colorado Cancer Center, Aurora, CO 80045

Submitted December 30, 2005; Revised August 30, 2006; Accepted September 7, 2006
Monitoring Editor: Marianne Bronner-Fraser

**Repellents evoke growth cone turning by eliciting asymmetric, localized loss of actin cytoskeleton together with changes in substratum attachment. We have demonstrated that semaphorin-3A (Sema3A)-induced growth cone detachment and collapse require eicosanoid-mediated activation of protein kinase Cε (PKCε) and that the major PKCε target is the myristoylated, alanine-rich C-kinase substrate (MARCKS). Here, we show that PKC activation is necessary for growth cone turning and that MARCKS, while at the membrane, colocalizes with $\alpha_3$-integrin in a peripheral adhesive zone of the growth cone. Phosphorylation of MARCKS causes its translocation from the membrane to the cytosol. Silencing MARCKS expression dramatically reduces growth cone spread, whereas overexpression of wild-type MARCKS inhibits growth cone collapse triggered by PKC activation. Expression of phosphorylation-deficient, mutant MARCKS greatly expands growth cone adhesion, and this is characterized by extensive colocalization of MARCKS and $\alpha_3$-integrin, resistance to eicosanoid-triggered detachment and collapse, and reversal of Sema3A-induced repulsion into attraction. We conclude that MARCKS is involved in regulating growth cone adhesion as follows: its nonphosphorylated form stabilizes integrin-mediated adhesions, and its phosphorylation-triggered release from adhesions causes localized growth cone detachment critical for turning and collapse.**

## INTRODUCTION

The nerve growth cone is the amoeboid tip of the developing neurite. It navigates through the extracellular milieu by integrating molecular signals and translating them into changes of direction or speed. To respond to directional cues, the growth cone must regulate the distribution and magnitude of traction forces generated against the growth substratum (Suter and Forscher, 2000). Repellents (i.e., negative chemotropic agents) are thought to evoke the turning response by eliciting asymmetric collapse (Fan and Raper, 1995) characterized by rapid loss of growth cone area, loss of the peripheral actin cytoskeleton, and concomitant release from the substratum (Mikule *et al*., 2002). Many recent studies are focused on how guidance cues control the actin cytoskeleton via Rho-family GTPases and their effectors (Huber *et al*., 2003). In contrast, control of adhesion, which is the main topic of this report, has received less attention.

Data on cell–matrix adhesions come primarily from studies of focal contacts, protein complexes that link actin stress fibers across the plasma membrane to the extracellular matrix (Jockusch *et al*., 1995). However, growth cones and highly motile cells lack focal contacts and rely on less prominent, more dynamic adhesions (Gundersen, 1988; Lee and Jacobson, 1997). Some of the proteins found in focal contacts also have been identified within growth cones (Letourneau and Shattuck, 1989; Cypher and Letourneau, 1991; Arregui *et al*., 1994; Schmidt *et al*., 1995; Renaudin *et al*., 1999), but the molecular composition of growth cone adhesions and their dynamic regulation remain poorly understood.

The growth cone's response to repellents requires regulated detachment from the growth substratum. Although the signaling cascades initiated by many classes of repellent have been characterized and are known to affect actin cytoskeletal dynamics, the mechanisms by which they affect assembly and disassembly of adhesion complexes are largely unknown. Semaphorin-3A (Sema3A) is a prototypical secreted repellent required for proper patterning of the developing nervous system (Messersmith *et al*., 1995). Sema3A-induced growth cone collapse requires activation of the Rho-family GTPase Rac1 (Jin and Strittmatter, 1997) and LIM-kinase (Aizawa *et al*., 2001), which regulate actin cytoskeleton dynamics (Gungabissoon and Bamburg, 2003). Several lines of evidence support the argument that Sema3A signaling targets adhesions via eicosanoid activation of pro-

This article was published online ahead of print in *MBC in Press* (http://www.molbiolcell.org/cgi/doi/10.1091/mbc.E05–12–1183) on September 20, 2006.

† These authors contributed equally to this work.

* Present address: Department of Biology, University of North Carolina, Chapel Hill, NC 27599.

Address correspondence to: Karl H. Pfenninger (karl.pfenninger@uchsc.edu).

Abbreviations used: Bis, bisindolylmaleimide I; DRG, dorsal root ganglion; ED, effector domain; GCP, growth cone particle; 12(*S*)-HETE, 12(*S*)-hydroxyeicosatetraenoic acid; IRM, interference reflection microscopy; MARCKS, myristoylated alanine-rich C-kinase substrate; PAZ, peripheral adhesive zone; P-MARCKS, MARCKS phosphorylated in the ED; Sema3A, semaphorin 3A; TPA, 12-*O*-tetradecanoyl-phorbol-13-acetate.

tein kinase C (PKC)ε. Growth cones treated with lipoxygenase inhibitor that are thus unable to generate 12(*S*)-hydroxyeicosatetraenoic acid [12(*S*)-HETE] remain spread out and attached to the substratum even after significant Sema3A-induced loss of F-actin (Mikule *et al*., 2002). Likewise, induction of growth cone collapse by thrombin, which requires 12(*S*)-HETE (de la Houssaye *et al*., 1999) and PKC activity (Mikule *et al*., 2003), targets growth cone adhesions independently of its effects on the actin cytoskeleton. Biochemical analyses of isolated growth cones and functional studies of dorsal root ganglion (DRG) growth cones demonstrate that the lipoxygenase product 12(*S*)-HETE directly and selectively activates PKCε (Mikule *et al*., 2003). Based upon these data, we hypothesized that the repellents Sema3A and thrombin (and possibly Sema4D; Barberis *et al*., 2004) activate signaling pathways that affect growth cone adhesion sites via eicosanoid-mediated activation of PKCε. A likely candidate effector of this activation is myristoylated, alanine-rich C-kinase substrate (MARCKS), the primary PKCε substrate in the growth cone (Mikule *et al*., 2003).

In the growth cone, MARCKS is abundant (Katz *et al*., 1985; Mikule *et al*., 2003), and it is the only known protein whose phosphorylation is stimulated by 12(*S*)-HETE (Mikule *et al*., 2003). MARCKS has been implicated in regulating cell attachment and spreading (Manenti *et al*., 1997; Myat *et al*., 1997; Disatnik *et al*., 2002, 2004; Iioka *et al*., 2004; Calabrese and Halpain, 2005), and it colocalizes with adhesion complexes in cultured cells (Rosen *et al*., 1990; Berditchevski and Odintsova, 1999). Membrane association of MARCKS is regulated, in part, by PKC phosphorylation of serine residues within its "effector domain" (ED; McLaughlin and Aderem, 1995). The ED cross-links actin, binds $Ca^{2+}$/calmodulin, and interacts with negatively charged membrane phospholipids (e.g., phosphatidylinositol bisphosphate; Laux *et al*., 2000). Negative charge introduced to the ED by PKC phosphorylation causes MARCKS to dissociate from the membrane (Thelen *et al*., 1991; Kim *et al*., 1994). ED phosphorylation also inhibits the ability of MARCKS to bind $Ca^{2+}$/calmodulin (Hartwig *et al*., 1992), and via conformational change, to cross-link F-actin (Bubb *et al*., 1999). Although the role of the ED in regulating the dynamic association of MARCKS with the plasma membrane is well documented, the ED is not required for its punctate distribution at the membrane. Thus, the interaction of other MARCKS domain(s) with membrane components seems likely (Swierczynski and Blackshear, 1995; Seykora *et al*., 1996; Blackshear *et al*., 1997; Laux *et al*., 2000). Interestingly, MARCKS seems to be necessary for normal patterning of the nervous system as MARCKS null mice (Stumpo *et al*., 1995; Blackshear *et al*., 1997) exhibit phenotypic abnormalities that include complete agenesis of forebrain commissures, neuronal ectopia, and severe midline defects. Although there are several possible mechanisms of pathogenesis, defects in MARCKS-dependent cell adhesion or spreading may explain these phenotypes.

The observations summarized here led us to investigate the possibility that MARCKS functions as a dynamic regulator of adhesion during growth cone pathfinding. Specifically, we hypothesized that nonphosphorylated MARCKS stabilizes integrin-mediated adhesion of growth cones and that Sema3A-induced MARCKS phosphorylation causes the dissociation of adhesions and detachment necessary for turning and collapse responses. These hypotheses were tested in biochemical experiments and in MARCKS gain- and loss-of-function studies.

## MATERIALS AND METHODS

### *Materials*

The culture supernatant of stably transfected human embryonic kidney (HEK)293 cells secreting Sema3A (generous gift from Dr. M. Tessier-Lavigne, Genentech, Inc., South San Francisco, CA) was concentrated by ultrafiltration (Centriplus membrane, 50,000-mol. wt. cut-off; Millipore, Billerica, MA). Sema3A concentration was calibrated by comparing the degree of collapse response to that of a known standard. Special reagents and their sources were 12(*S*)-HETE (BIOMOL Research Laboratories, Plymouth Meeting, PA); bisindolylmaleimide I (Bis) and 12-*O*-tetradecanoyl-phorbol-13-acetate (TPA) (EMD Biosciences/Calbiochem, San Diego, CA); culture media, media supplements, and TRIzol reagent (Invitrogen, Carlsbad, CA); GC-Melt, EGFP-N1 vector, and pIRES-GFP vector (Clontech, Mountain View, CA); and small interfering RNAs (siRNAs) (Dharmacon RNA Technologies, Lafayette, CO). Antibody specificities and their sources were $\alpha_3$-integrin (developed by L. Reichardt, University of California, San Francisco, CA) (Developmental Studies Hybridoma Bank, maintained under the auspices of the National Institute of Child Health and Human Development by Department of Biological Sciences at the University of Iowa, Iowa City, IA); MARCKS (antibody used for Western blots) and lamin A and C (Santa Cruz Biotechnology, Santa Cruz, CA); MARCKS (antibody used for immunofluorescence and blot in Supplemental Figure 1) (Proteintech Group, Chicago, IL); $\beta_1$-integrin and PKCε (BD Biosciences, Franklin Lakes, NJ); MARCKS phosphorylated in the ED (P-MARCKS) (Cell Signaling Technology, Beverly, MA); and tubulin β III (Abcam, Cambridge, MA). Additional chemicals, unless stated otherwise, were from Sigma-Aldrich (St. Louis, MO) and of the highest quality available.

### *Growth Cone Isolation*

Growth cone particles (GCPs) were prepared as described previously (Pfenninger *et al*., 1983; Lohse *et al*., 1996). Briefly, whole brains from fetal rats (18-d gestation) were homogenized in 0.32 M sucrose containing 1 mM $MgCl_2$, 2 mM TES buffer, pH 7.3, and 2 μM aprotinin. Low-speed (1660 × *g* for 15 min) supernatant of the homogenate was layered onto a discontinuous density gradient (0.83 and 2.66 M sucrose containing 1 mM $MgCl_2$ and 2 mM TES) and spun to equilibrium at 242,000 × *g* at 4°C for 40 min in a vertical rotor (VTi50; Beckman Coulter, Fullerton, CA). GCPs at the 0.32/0.83 M sucrose interface were collected, diluted with ~5–10 volumes 0.32 M sucrose buffer, pelleted (40,000 × *g* for 30 min), and then resuspended in an appropriate buffer depending upon subsequent experimentation.

### *MARCKS Phosphorylation and Translocation Assays*

Pelleted GCPs (60–100 μg of protein per reaction) were resuspended in 100 μl of ice-cold kinase buffer (20 mM HEPES, pH 7.0, 10 mM $MgCl_2$, and 1 mM EGTA; Mikule *et al*., 2003). Effectors were added; after 10 min on ice, reaction mixtures were incubated at 30°C for 2 min and then chilled on ice. In experiments with PKC inhibitor, 10 nM Bis was added 10 min before the effector. Samples were homogenized (Teflon-glass) and separated into particulate (membrane/cytoskeleton) and cytosolic fractions by centrifugation at 100,000 × *g* for 30 min at 4°C. The resulting pellets were solubilized in 20 μl of 5% SDS. Protein in supernatant fractions was precipitated with chloroform/methanol, and these pellets also were solubilized in 5% SDS. After addition of Laemmli sample buffer, polypeptides of all samples were resolved by SDS-PAGE, blotted, and probed with antibody to MARCKS or to P-MARCKS (see below).

### *Gel Electrophoresis and Western Analysis*

Polypeptides were resolved by SDS-PAGE along side with dual-colored Precision Plus Protein standards (Bio-Rad, Hercules, CA). Blots were prepared by wet electrotransfer (Towbin *et al*., 1979) to a polyvinylidene difluoride membrane (Immobilon P; Millipore). They were blocked in Tris-buffered saline (TBS) with 5% nonfat evaporated milk and 0.1% Tween 20 for at least 2 h at room temperature. After quenching, blots were incubated in blocking buffer containing primary antibodies for 1 h, rinsed (three times) in the same buffer, and incubated in blocking buffer containing Cy5-conjugated secondary antibody (Invitrogen), rinsed (three times) in TBS/Tween, and then scanned using a Typhoon 9400 multi-mode imager (GE Healthcare, Little Chalfont, Buckinghamshire, United Kingdom).

### *Cloning, Vector Construction, and Small Interfering RNA (siRNA)*

Total RNA was isolated from fetal rat brain (18-d gestation) by using TRIzol reagent. cDNA encoding rat MARCKS was generated by reverse transcriptase-polymerase chain reaction (RT-PCR) by using the purified RNA, Ready-To-Go RT-PCR beads (PerkinElmer Life and Analytical Sciences, Boston, MA), and the following primers: forward, 5′-ccgctcgagatgggtgcattctcc-3′ and reverse, 5′-cccaagcttctcggccaccggcgcgg-3′.

Due to the high gc-content of these primers and of MARCKS, we added GC-Melt during the PCR cycles. The RT-PCR product was then ligated into the EGFP-N1 vector. Plasmid containing the MARCKS-ED mutant was a

generous gift from Dr. Alan Aderem (Institute for Systems Biology, Seattle, WA). The coding sequence for MARCKS-ED was excised and subcloned into the bicistronic pIRES-GFP vector, which expresses both the inserted protein and green fluorescent protein (GFP) (for the identification of neurons expressing mutant MARCKS) under the control of the cytomegalovirus promoter. Coexpression was confirmed in transfected HEK293 cells by indirect immunofluorescence microscopy (our unpublished data). Correctness of all constructs was established using restriction digests and Big Dye sequencing (Barbara Davis Center for Childhood Diabetes, DNA Sequencing Core, University of Colorado at Denver and Health Sciences Center, Aurora, CO).

Rat MARCKS siRNA was custom synthesized by the SMARTPool siRNA design service of Dharmacon RNA Technologies. The lamin A and C control siRNA also was purchased from Dharmacon RNA Technologies. The pmaxGFP plasmid used for cotransfection was purchased with the Nucleofector kit (Amaxa Biosystems, Gaithersburg, MD).

### Neuron Culture and Transfection

For explant cultures, dorsal root ganglia (DRGs) were dissected from 15-d gestation Sprague-Dawley rat fetus and cultured on laminin-coated coverslips (Assistent brand) in B27/Neurobasal medium supplemented with 10% (vol/vol) fetal bovine serum (FBS) and 100 ng/ml nerve growth factor (NGF). For some of the collapse assays shown in Figure 1, we also used poly-D-lysine (polylysine)-coated coverslips for culture. After 24-h incubation at 37°C, 4% $CO_2$ in air, this medium was replaced with fresh B27 medium without other supplementation. After a second day in culture, neurites with spread growth cones were used for turning assays and indirect immunofluorescence experiments as described below.

For experiments requiring transfection, excised DRGs from 10 to 12 fetal rats were dissociated. In some cases, 5 mg/ml dispase and 1 mg/ml collagenase in modified Hank's balanced salt solution were used first (25 min at 37°C). The partially digested or the fresh ganglia were pelleted, and the supernatant was replaced with trypsin/EDTA. After 15 min, ganglia were washed in B27 medium with serum, triturated, and cells were counted. Dissociated cells ($2–3 \times 10^6$) were pelleted and resuspended in 100 $\mu$l of Nucleofector solution (Amaxa) with 5 $\mu$g of DNA or 0.4 $\mu$M siRNA plus 2.5 $\mu$g of pmaxGFP (Amaxa) and electroporated using the Amaxa Nucleofector device per the manufacturer's instructions (setting O-003). Transfected neurons were cultured on laminin in B27 medium with FBS and NGF, replaced every 24 h. Experimentation was conducted in the presence of both FBS and NGF.

Knockdown of MARCKS expression in neurons could not be assessed by Western blot because the transfection efficiency was only ~30% in these cultures. However, growth cone MARCKS immunofluorescence shown in Figure 6 is represented at exactly the same enhancement and contrast levels so that direct comparisons are possible.

### Growth Cone Turning Assays

Sema3A gradients were generated in the proximity of cultured nerve growth cones by repetitive pulse application (Lohof *et al*., 1992). Micropipettes (inner tip diameter consistently 1–2 $\mu$m) were connected to a Picospritzer (set at 6 psi; General Valve, Fairfield, NJ) controlled by a square wave generator (2 Hz, duration 10 ms; Astro-Med, West Warwick, RI). The system was calibrated by generating a model gradient of fluorescein-conjugated dextran. Such gradients proved reproducible and stable over time.

For turning assays, culture coverslips were placed in an open chamber with medium, layered over with inert mineral oil (embryo tested, sterile filtered; Sigma-Aldrich) to avoid evaporation and maintain pH, and observed on the microscope stage under convective heating at a constant 37°C. For interference reflection microscopy (IRM) imaging, we additionally used an objective heater (set at 36°C) in conjunction with the oil immersion lens. At the start of each experiment, the tip of the factor-loaded micropipette was positioned 100 $\mu$m away from the selected growth cone, at an angle 45° from the initial direction of growth cone advance (as determined by the orientation of the growth cone's neurite shaft). Initiation of factor expulsion marked the start (time t = 0) for each experiment. Phase-contrast images were captured at 5-min intervals over the course of 1 h. To be scored, growth cones had to advance a minimal distance of at least twice their original length. Once this criterion had been met, growth cones were tracked for 1 h or until they either stopped (i.e., no advancement for ≥10 min) or branched. Statistical significance of final turning angles was determined using Student's *t* test (assuming equal variances). For sequences involving IRM, micrographs were acquired at 1- or 2-min intervals for 30–45 min.

### Microscopy

All images were acquired using a Zeiss Axiovert 200M microscope equipped with Zeiss optics, a Cooke Sensicam digital camera, and Slidebook software (Intelligent Imaging Innovations, Denver, CO). The following objective lenses were used: Zeiss Plan-Apochromat 63×/1.4 oil for epifluorescence and IRM; Zeiss Plan-NeoFluar 63×/1.25 oil for phase contrast. To generate digitally deconvolved images, we applied the nearest neighbor algorithm of Slidebook to images taken at 0.2- to 0.3-$\mu$m intervals through the sample. Images shown are from the first optical slice exhibiting fluorescence as the plane of focus moved from the coverslip into the growth cone. Images were adjusted for brightness and contrast with Adobe Photoshop software (Adobe Systems, Mountain View, CA). However, fluorescence levels are shown so they can be compared (see above), unless indicated otherwise. For IRM, optics were calibrated by acquiring color images with a tunable RGB filter (CRI MicroColor, Cambridge, MA) to identify and minimize contributions from higher order interference. To objectively determine growth cone close contact area, mean intensity of a 100 × 100 pixel region near the growth cone was measured as background using MetaMorph software (Molecular Devices, Sunnyvale, CA). IRM images were thresholded to include only pixels with intensities less than 2 SDs below the mean background intensity of the 100 × 100 pixel region. The area of thresholded pixels within the periphery of the growth cone was then determined and reported as adhesive or close contact area.

### Growth Cone Collapse Assays

DRG neurons on laminin-coated coverslips were placed under a convective heater on the microscope stage as described above. Factors were introduced into the medium with a syringe and needle, and images were acquired at specific intervals thereafter. The thresholding function in Slidebook was used to measure growth cone areas. Student's *t* test (assuming equal variances) was used to determine statistical significance of observed differences.

### Fixation and Labeling of Growth Cones in Culture

DRG cultures were fixed using slow infusion of 4% (wt/vol) formaldehyde in 0.1 M phosphate buffer, pH 7.4, with 120 mM glucose and 0.4 mM $CaCl_2$, as developed for electron microscopy (Pfenninger and Maylie-Pfenninger, 1981). Cultures were rinsed (three times) with phosphate-buffered saline (PBS) containing 1 mM glycine, permeabilized with blocking buffer [PBS, 1% (wt/vol) bovine serum albumin] plus 1% (vol/vol) Brij 98 detergent for 2 min at room temperature, and placed in blocking buffer for 1 h at room temperature. Quenched cultures were incubated with primary antibody at 1:100 dilution in blocking buffer, for 1 h at room temperature, and washed (three times) with blocking buffer. This process was repeated with Alexa Fluor 488- (green), 594- (red), or Marina-blue (blue)-conjugated secondary antibodies (Invitrogen) at the same dilution. In some experiments that required dual fluorescence labeling of antigens in GFP-expressing growth cones, we used secondary antibodies conjugated to Alexa Fluor 594 and 647. Coverslips were mounted on slides by using a polyvinyl alcohol/glycerol medium containing *n*-propyl gallate as antifade reagent.

We made significant efforts to generate IRM and immunofluorescence images from the same growth cones. However, even very mild fixation with 1% formaldehyde or 0.1% glutaraldehyde at 4°C for as little as 60 s, followed by immediate quenching of aldehyde groups, resulted in extensive artifactual "close contacts" that covered most of the growth cone area. Thus, it seemed that even minimal protein cross-linking, needed for growth cone preservation and labeling, altered the IRM images significantly so that colocalization of close contacts with integrins and/or MARCKS in the same growth cone was impossible.

### Colocalization Analysis and Morphometry

Digitally deconvolved (nearest neighbor) images of growth cones were analyzed using ImageJ software (National Institutes of Health, Bethesda, MD). To exclude contributions of background noise in an unbiased manner, we proceeded in two ways: 1) We thresholded all images by limiting the eight-bit display range to 10–255 and calculated Manders' coefficient (R) by using the Manders' coefficient plug-in. 2) Alternatively, we performed automatic threshold calculation in conjunction with overlap analysis (Manders' coefficient $R_T$) according to Costes *et al*. (2004). For this, we used the "Colocalization Threshold" plug-in (see the ImageJ Web site established by the Wright Cell Imaging Facility, Toronto Western Research Institute, Toronto, Ontario, Canada; www.uhnresearch.ca/wcif). In both cases, zero/zero pixels were excluded from the quantitation.

## RESULTS

### Growth Cone Turning and Collapse Involves Regulation of Adhesion

Reduction in growth cone close contacts, seen as IRM-dark structures, is an important step of, and actually precedes, growth cone collapse (Mikule *et al*., 2002). These experiments, like virtually all of our previous studies on growth cone behavior, were done on laminin, a substratum to which growth cones attach in a regulated manner via integrins. If regulation of growth cone adhesion is necessary for collapse, as we propose, then growth cones adhering nonspecifically to a substratum should be collapse-inhibited. Therefore, we measured Sema3A-induced collapse responses of DRG

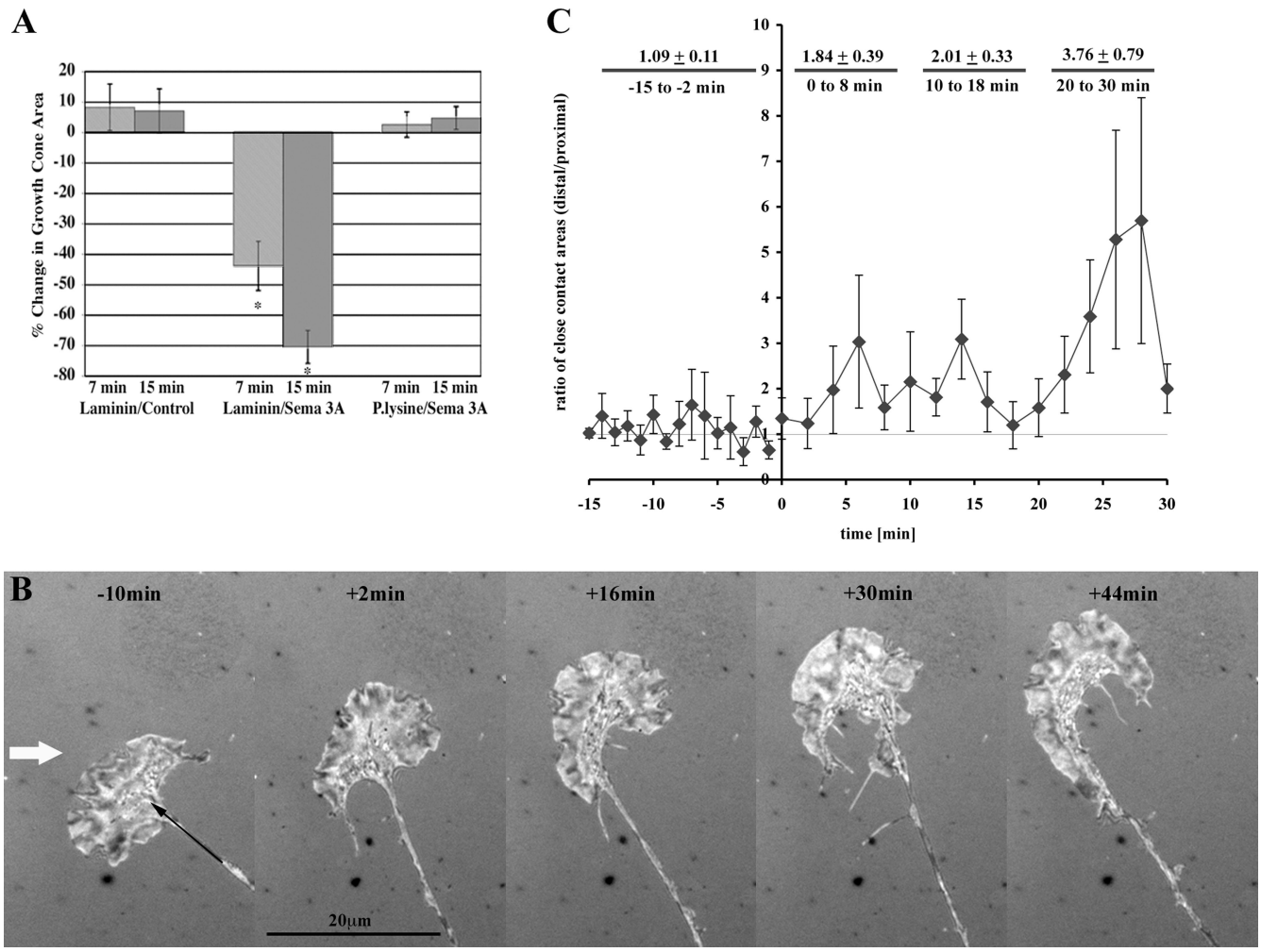


**Figure 1.** Role of adhesion in growth cone repulsion. (A) Effect of the substrate on Sema3A-mediated growth cone collapse. Growth cones of DRG neurons were cultured either on laminin- or polylysine-coated surfaces. Phase contrast micrographs were taken just before, and at 7 and 15 min after, Sema3A addition to the culture medium. Growth cone areas were measured, and percentage of change was calculated. *$p < 2 \times 10^{-4}$ compared with laminin/control or polylysine/Sema3A. For control, n = 21; for Sema3A/laminin, n = 11; and for Sema3A/polylysine, n = 10. (B and C) Redistribution of IRM-dark growth cone adhesions during turning in a microgradient of Sema3A. DRG growth cones on laminin. (B) IRM pictures were taken at the indicated times. The white arrow shows the orientation of the micropipette tip (100 $\mu$m away) during the experiment. The black arrow shows the neurite and growth cone axis. (C) Quantitative analysis of close contact area proximal versus distal to the Sema3A gradient, relative to the growth cone axis. This axis was determined for each frame analyzed. Data are from five growth cones. Four of these cones were observed for the entire 45-min experiment, including 15 min before generation of the gradient (time = 0). A fifth control was added to the −15- to 0-min data. The thin horizontal line indicates a ratio of 1.0. The numbers on the top are the average ratios ± SEM for the indicated intervals.

growth cones on polylysine and compared them with those of growth cones adhering to laminin. To quantify collapse, growth cone area was measured before, and 7 and 15 min after, challenge (Mikule *et al*., 2002). Figure 1A shows the expected reduction in growth cone area on laminin (Mikule *et al*., 2002). In contrast, growth cones on polylysine did not collapse at all for at least 15 min after Sema3A challenge. Thus, a physiological substrate that allows for integrin affinity regulation, such as laminin, seems to be necessary for growth cone collapse. Because motility involves cycles of adhesion and detachment, this result is consistent with our finding that growth cones advance much more slowly on polylysine than on laminin (Wang and Pfenninger, 2006).

This observation raised the issue of whether growth cone adhesions undergo redistribution when asymmetrically exposed to a repellent. We addressed this question by IRM imaging DRG growth cones in the presence of a microgradient of Sema3A (Lohof *et al*., 1992). In IRM regions of close contact (i.e., adhesions) look dark, whereas intermediate areas look lighter than background (Izzard and Lochner, 1976). As shown in Figure 1B, the initially more or less symmetrical distribution of close contacts (relative to the growth cone axis, defined as the neurite's extension; black arrow) became progressively asymmetric, shifting away from the repellent source (micropipet 100 $\mu$m away; orientation indicated by white arrow). To quantify this shift, we analyzed IRM time-lapse movies of growth cones responding to Sema3A gradients. Data were expressed as the ratios of aggregate close contact areas on either side of the growth cone axis (distal/proximal relative to the repellent source). The growth cone axes were redefined for each successive frame/time point as the growth cones turned and the neurites changed direction. This enabled us to assess adhesion asymmetry for each time point. Four of the five growth

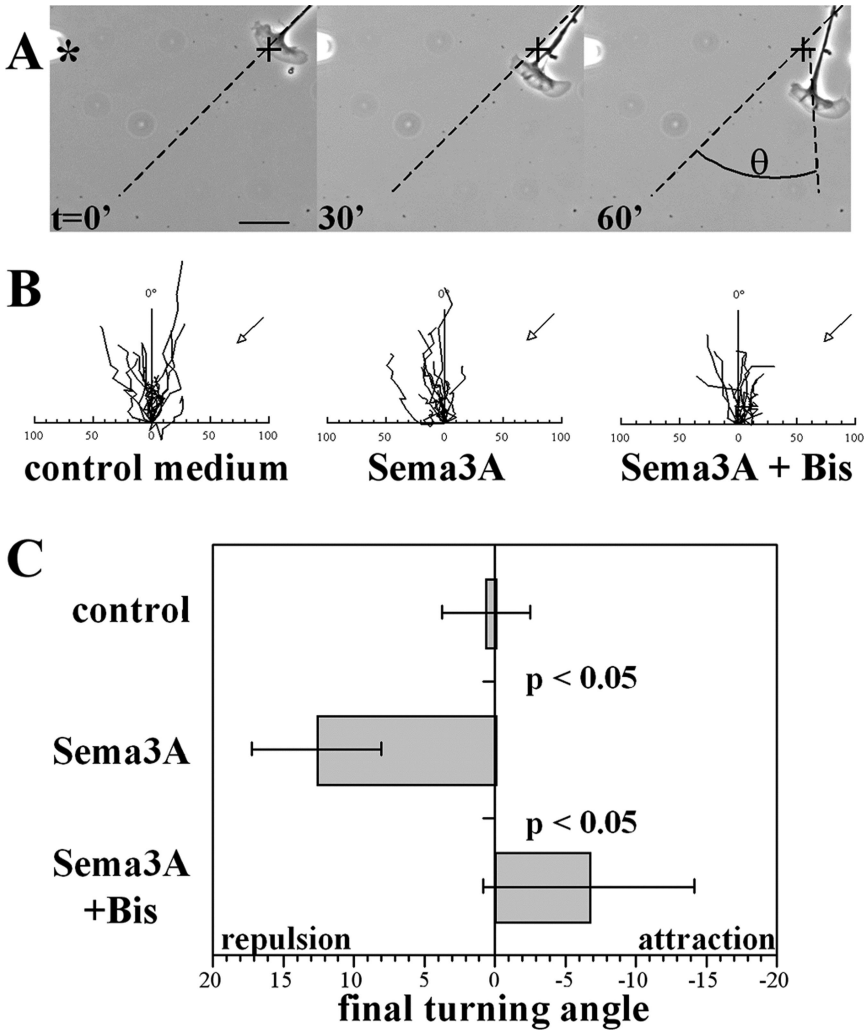


**Figure 2.** Effect of PKC inhibition on Sema3A-induced turning. Growth cones of DRG neurons (on laminin) were exposed to gradients of control medium or of Sema3A. (A) Phase contrast micrographs of a growth cone in a Sema3A gradient, taken at 30-min intervals. The first panel demonstrates the relative positions of the growth cone (+) and the micropipette tip (*) at the start of the experiment. In the third panel, $\theta$ is the final turning angle (see below). Bar, 20 $\mu$m. (B) Rosebud plots depicting 1-h traces of axonal growth cone translocation in control and Sema3A gradients. Sema3A experiments also were conducted in bath medium with the PKC inhibitor Bis (1 $\mu$M). Arrows mark the location of the micropipette tip. Abscissa scale is in micrometers. (C) Rosebud data were analyzed by measuring the final turning angles for each 1-h experiment, mean final turning angles ± SEM. The p values compare control to Sema3A, and Sema3A to Sema3A plus Bis, respectively.

cones analyzed in the gradient (plus an additional control) were observed for 15 min before Sema3A application. During this time, their close adhesions shifted around the growth cone axis only moderately and apparently at random, and the ratio averaged 1.09 ± 0.11 (mean ± SEM). On Sema3A gradient formation (starting at time 0), the distribution of close adhesions changed and fluctuated substantially (Figure 1B). Ratio values increased to 3.0 but returned again to below 2.0 (Figure 1C), in part because of neurite reorientation. Overall, however, close adhesions moved away from the repellent source. The average ratios increased progressively over time, from 1.09 for the controls to 1.84 ± 0.39 for the first 8 min in the gradient (not significantly different; $p = 0.07$), to 2.01 ± 0.33 for the 10- to 18-min interval (significantly above control; $p < 0.02$) and to 3.76 ± 0.79 for the 20- to 30-min interval ($p < 0.005$). Had we not redefined the growth cone axis for each frame, the close adhesion ratio rapidly would have reached much higher levels (moreover, the ratio for two of the five growth cones reached infinity within 8 and 14 min after gradient application). These IRM experiments indicated that the application of a repellent gradient caused rapid changes in the distribution of the growth cone's close adhesions, resulting in their progressive shift away from the repellent source. Overall, our observations show that regulation of adhesion is a critical step in growth cone collapse and turning, and they raise the question of which mechanisms are involved in these rapid adhesion changes.

### *PKC Activity Is Necessary for Sema3A-induced Repulsion*

We have shown that the repellents thrombin and Sema3A trigger growth cone collapse via a cascade that requires activation of PKC (Mikule *et al*., 2002). To test the hypothesis that Sema3A-induced repulsion, a far more complex growth cone response, also requires PKC activity, we generated microgradients of Sema3A in the proximity of growth cones of DRG neurons in culture, in the presence or absence of the PKC inhibitor Bis. At the concentration used, Bis is a selective inhibitor of the PKC isozymes $\alpha$, $\beta$I, $\beta$II, and, notably, $\varepsilon$ (Toullec *et al*., 1991). The response of growth cones to Sema3A microgradients was quantitatively assessed by tracking their positions over time, and the results were represented in rosebud plots (Figure 2B) and as final turning angles (Figure 2C). To determine the latter, we measured the angle formed between the original axis of outgrowth of the growth cone and a line drawn from the growth cone's initial position (corresponding to the origin of the rosebud plot) to its final position (Figure 2A). The paths of growth cones exposed to control gradients (conditioned medium from HEK293 cells not producing Sema3A) exhibited a symmetric distribution about the *y*-axis (Figure 2B, control medium), indicating that the control medium had no

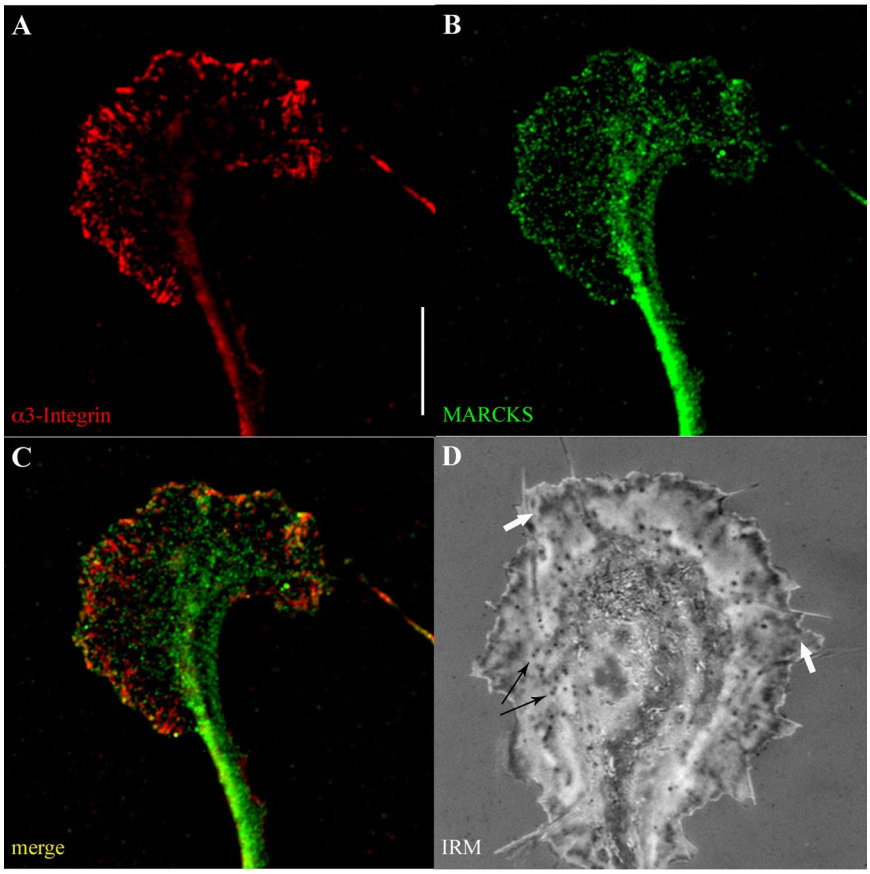


**Figure 3.** Localization of MARCKS, $\alpha_3$-integrin, and adhesions within the growth cone. (A–C) Digitally deconvolved fluorescence micrographs of a DRG growth cone cultured on laminin. The growth cone has been double-labeled with antibodies against $\alpha_3$-integrin and MARCKS. (C) The merged image (overlap in yellow). (D) IRM image of a DRG growth cone cultured on laminin. White arrows point at the PAZ (dark); black arrows mark putative point contacts. Bar, 10 $\mu$m.

effect on growth cone turning, as expected. This observation was reflected in the corresponding average final turning angle of about 0° (Figure 2C, control). In contrast, exposure to gradients of Sema3A caused almost all growth cones to turn away from the micropipette releasing the repellent (Figure 2, A and B). The final average turning angle was 12 ± 4° (Figure 2C). In the presence of Bis, however, the turning response was completely abrogated (Figure 2, B and C). In the rosebud plot representing these experiments, it seems as though extension rates of axons were reduced. Examination of individual tracks revealed that shorter growth cone paths resulted from increased instances of growth cone collapse or branching, which terminated the assay (our unpublished data; see *Materials and Methods*). The critical result of the Sema3A/Bis experiments was that, in the presence of the PKC inhibitor, the final turning angle was not significantly different from that observed in control conditions (Figure 2, B and C). These results demonstrate that a Bis-sensitive kinase activity is necessary for growth cone turning induced by Sema3A.

### *MARCKS Is a Component of Functional Growth Cone Adhesions*

MARCKS is the primary substrate of 12(*S*)-HETE-activated PKCε in the growth cone (Mikule *et al.*, 2003). If MARCKS is involved in regulating the growth cone's adhesions, then it most likely localizes to adhesive areas. We tested this hypothesis by immunolocalization with antibodies to MARCKS and to $\alpha_3$-integrin, a component of the laminin-binding $\alpha_3\beta_1$-integrin heterodimer (neurons were grown on laminin). Antibodies were tested for specificity by Western blot. The $\alpha_3$-integrin antibody used for immunofluorescence microscopy works in such blots only in nonreducing conditions. It labels a single band that comigrates with $\beta_1$-integrin just above the 250-kDa marker, at the $M_r$ expected for the heterodimer (Supplemental Figure 1). On reduction, the $\beta_1$-integrin antibody recognizes a single band at ~120 kDa. The specificity of the MARCKS antibodies used also is shown in Supplemental Figure 1. For immunolocalization, we isolated the optical sections containing the adhesive plane of DRG growth cones by using digital deconvolution. As shown in Figure 3, A–C, both proteins exhibited punctate distributions, which were consistent with those observed for other putative growth cone adhesion molecules (Arregui *et al.*, 1994; Renaudin *et al.*, 1999; Mikule *et al.*, 2002, 2003). MARCKS immunoreactivity was present in the central growth cone domain, whereas $\alpha_3$-integrin puncta were noticeably sparse. However, the densities of both increased toward the growth cone periphery, with overlap (yellow) evident in an irregular, band-like region along the growth cone edge.

Integrin $\alpha_3$/MARCKS overlap was analyzed quantitatively in digitally deconvolved images that included the growth cone's adhesive plane. By using two different, unbiased thresholding approaches (see *Materials and Methods*) to calculate Manders' coefficients for either the combined channels or for each channel separately, we analyzed the whole growth cone and two specific regions near its edge. These areas consisted of a band, 1 $\mu$m in width, running along the plasma membrane, and a second band, 2 $\mu$m in width and immediately proximal to the first (labeled PAZ, for peripheral adhesive zone, and proximal, respectively, in Figure 4A, top; for further explanation, see below). The sizes of the areas sampled are listed in Table 1, together with Manders' coefficients. R values range from 0 to 1, indicating no or complete overlap, respectively. The values of R are influenced by the channel ratio, and, to be

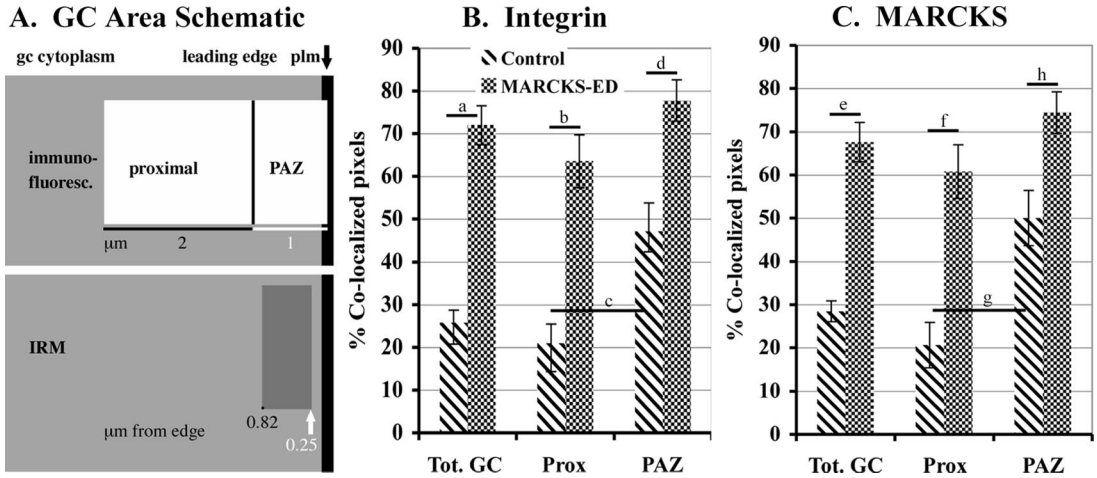


**Figure 4.** (A) Schematic of the growth cone's leading edge (plm, plasma membrane; gc, growth cone). Top (immunofluorescence), areas measured for colocalization analysis. Bottom (IRM), location of IRM-dark PAZ. (B and C) Results of colocalization analysis by using automatic threshold determination according to Costes *et al*. (2004). Graphs show, separately for each channel ($\alpha$3-integrin and MARCKS), the number of pixels that had both channel intensities above threshold, expressed as percentage of the total number of pixels above threshold (means ± SEM). Values are based on the results for $R_T$ shown in Table 1. Student's *t* tests were performed to assess the significance of differences between values. The lowercase letters refer to the p values: a and e, $<5 \times 10^{-7}$; b, $<5 \times 10^{-5}$; c, <0.005; d and g, <0.002; f, $<10^{-4}$; and h, <0.01.

reliable, should be near 1.0. As shown in Table 1, this was indeed the case. The presumably more stringent thresholded overlap coefficients, $R_T$, also are shown in Table 1, separately for each channel. For the whole growth cone and the proximal

**Table 1.** Colocalization of $\alpha_3$-integrin and MARCKS

| Area/experiment[a] | Thresholded colocalization coefficient ($R_T$)[b] | | Manders' coefficient R[c] | Channel ratio[d] | Sample area ($\mu m^2$/growth cone) |
|---|---|---|---|---|---|
| | $\alpha_3$-Integrin | MARCKS | | | |
| Total growth cone | | | | | |
| Control | 0.229 ± 0.034 | 0.226 ± 0.033 | 0.475 ± 0.023 | 0.802 ± 0.029 | 240[e] |
| MARCKS-ED | 0.774 ± 0.057 | 0.714 ± 0.056 | 0.759 ± 0.045 | 0.856 ± 0.058 | 400[e] |
| PAZ | | | | | |
| Control | 0.463 ± 0.072 | 0.482 ± 0.072 | 0.674 ± 0.035 | 0.985 ± 0.034 | 12.6 ± 1.05 |
| MARCKS-ED | 0.820 ± 0.051 | 0.779 ± 0.054 | 0.833 ± 0.031 | 0.916 ± 0.025 | 17.7 ± 0.85 |
| Proximal | | | | | |
| Control | 0.200 ± 0.043 | 0.172 ± 0.046 | 0.444 ± 0.037 | 0.961 ± 0.042 | 24.4 ± 2.16 |
| MARCKS-ED | 0.669 ± 0.072 | 0.621 ± 0.073 | 0.762 ± 0.040 | 0.941 ± 0.034 | 35.4 ± 1.71 |
| p values[f] | | | | | |
| Total growth cone (C/M-ED) | $1.96 \times 10^{-7}$ | $5.44 \times 10^{-7}$ | $1.93 \times 10^{-5}$ | n.a. | n.a. |
| PAZ (C/M-ED) | $5.37 \times 10^{-4}$ | $3.10 \times 10^{-3}$ | $2.26 \times 10^{-3}$ | n.a. | n.a. |
| Proximal (C/M-ED) | $2.13 \times 10^{-5}$ | $4.63 \times 10^{-5}$ | $1.27 \times 10^{-5}$ | n.a. | n.a. |
| Control (PAZ/proximal) | $4.08 \times 10^{-3}$ | $1.43 \times 10^{-3}$ | $2.29 \times 10^{-5}$ | n.a. | n.a. |
| M-ED (PAZ/proximal) | $8.79 \times 10^{-2}$ | $8.54 \times 10^{-2}$ | $2.56 \times 10^{-3}$ | n.a. | n.a. |

n.a., not applicable.

[a] All images analyzed included the adhesive plane of the plasma membrane of the growth cone and were digitally deconvolved. For controls and for MARCKS-ED transfections, n = 9. Values are means ± SEM.

[b] Manders' colocalization coefficients for $\alpha$3-integrin (tM1; channel 1) and for MARCKS (tM2; channel 2), by using automatic threshold determination according to Costes *et al.* (2004). Zero/zero pixels were excluded. Manders' coefficients range from 0 (no overlap) to 1 (complete overlap). Corresponding values for percentage of pixels colocalized are shown in Figure 4.

[c] Manders' overlap coefficients for the combined channels. Zero/zero pixels were excluded. The weakest pixels were deleted in all images by limiting the eight-bit display range to 10–255.

[d] Channel ratios are shown because Manders' colocalization coefficient is based on the assumption that the ratio is close to 1. This is indeed the case, especially for PAZ and proximal areas.

[e] Approximate areas analyzed (values from Figure 7).

[f] Two-tailed Student's *t* tests were performed to assess statistical significance of 1) differences between controls and MARCKS-ED–transfected growth cones (C/M-ED) for the different areas, and 2) differences between PAZ and proximal areas (PAZ/proximal) in control and transfected growth cones. Except for the PAZ/proximal comparison of $R_T$ values in the growth cones transfected with M-ED, the differences were highly significant for either approach of colocalization analysis.

region, both R and $R_T$ values were quite low. However, for the PAZ they were much higher (Table 1). To make the meaning of these data more obvious, we also calculated the number of pixels that had both channel intensities above threshold, expressed as percentage of the total number of pixels above threshold (for each channel). These values are derivatives of $R_T$ (Table 1), and they are shown in Figure 4, B and C. For the whole growth cone or the proximal region, <30% of integrin-positive pixels also contained a MARCKS signal above threshold, and the corresponding values for MARCKS were comparable, as one would expect from the similar abundance of the two labels (Table 1, channel ratio). In the PAZ, however, these values were close to 50%, indicating significantly increased colocalization ($p < 0.005$). Thus, both analyses demonstrated a peripheral zone of substantial integrin/MARCKS colocalization, the growth cone's PAZ.

In complementary studies, IRM was used to visualize the close appositions (dark) of living DRG growth cones to their laminin-coated substratum. Figure 3D is a typical IRM image of a DRG growth cone on laminin. The adhesion patterns of different growth cones varied to some degree (Mikule *et al*., 2002), but certain characteristics were consistent: classical focal contacts (which are the dark regions in the shape of arrowheads and are associated with actin stress fibers) were absent from the highly motile growth cone. Instead, dark puncta (Figure 3D, black arrows; most likely point contacts; Arregui *et al*., 1994; Renaudin *et al*., 1999) were a prominent growth cone adhesive structure (when filopodia were present they typically contained such puncta). Additionally, growth cones possessed a more or less continuous band of close adhesion that followed their perimeter (Figure 3D, white arrows) as observed in other highly motile systems, such as fish scale keratocytes (Lee and Jacobson, 1997). This adhesive band was separated from the growth cone's distal edge by 0.25 ± 0.03 μm (mean ± SEM; n = 14, from at least 3 averaged measurements in 14 growth cones). Its proximal border reached on average 0.82 ± 0.05 μm into the growth cone (Figure 4A, bottom). Thus, this adhesive zone (the PAZ) spatially corresponded to the region of MARCKS–$\alpha_3$–integrin overlap (Figure 4A). (As explained in *Materials and Methods*, fixation altered the IRM images extensively and thus precluded the combined use of IRM and indirect immunofluorescence on the same growth cone.) The PAZ is reminiscent of a peripheral ribbon of attachment often observed in growth cones challenged with repellent in the presence of an inhibitor of 12/15(*S*)-HETE synthesis (see Figure 6 in Mikule *et al*., 2003). Such growth cones loose the radial actin cytoskeleton but may remain spread on the substratum, and the ribbon of attachment seems to correspond to the PAZ. The importance of these observations is that a subset of integrins, chiefly those colocalized with MARCKS, correlated spatially with close adhesions. This is consistent with a role of MARCKS in growth cone adhesion.

### *MARCKS Localization Depends upon Its Phosphorylation State*

It is well established in other biological systems that phosphorylation of MARCKS results in its dissociation from the membrane (Allen and Aderem, 1995; McLaughlin and Aderem, 1995). We knew that 12(*S*)-HETE stimulated PKCε and MARCKS phosphorylation in growth cones (Mikule *et al*., 2003), but we had not confirmed that this caused MARCKS translocation to the cytosol as in other systems. To address this issue, GCPs isolated from fetal rat brain were treated with or without 12(*S*)-HETE and fractionated into membranes (plus cytoskeleton) and cytosol. Polypeptides in the cytosolic and particulate fractions were resolved by SDS-PAGE and probed for MARCKS by Western blot. Stimulation of endogenous PKCε with 12(*S*)-HETE resulted in a substantial increase in cytosolic MARCKS (Figure 5A). This translocation was sensitive to Bis, suggesting that the observed effect was PKC dependent. We also wanted to demonstrate that cytosolic MARCKS was indeed phosphorylated. This was achieved by probing Western blots of experimental samples analogous to those just described with an antibody-specific for MARCKS phosphorylated in the ED (P-MARCKS). 12(*S*)-HETE increased P-MARCKS levels (by ~60%), and virtually all was recovered in the cytosol (Figure 5B). This is in stark contrast to the distribution of total MARCKS (Figure 5A), indicating a high ratio of P-MARCKS to total MARCKS in the cytosol versus a very low ratio in the particulate fraction. In conjunction with our earlier data, these results confirm in growth cones that 12(*S*)-HETE–

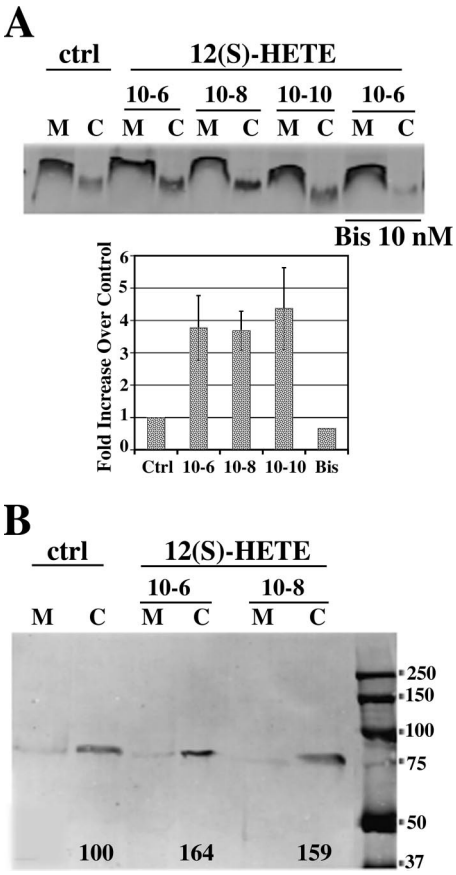


**Figure 5.** PKC-catalyzed phosphorylation and translocation of MARCKS within the growth cone. GCPs (equal amounts of protein per reaction) were either pretreated with vehicle alone or inhibitor (10 nM Bis) for 10 min before exposure to 12(*S*)HETE (2 min at 30°C) at the indicated concentrations. Reactions were quenched, and samples were fractionated into membranes (plus cytoskeleton; M) and cytosol (C). Western blots of fractions were probed with antibody to total MARCKS (A) or antibody specific for P-MARCKS (B). The amount of immunoreactivity in each fraction was determined using fluorescence intensity and compared with untreated controls. (A) Distribution of total MARCKS protein. Bar graph shows fold increase of cytosolic MARCKS over control (means ± SEM from 3 independent experiments). (B) Representative experiment of 12(*S*)-HETE-stimulated MARCKS phosphorylation (quantitative data in arbitrary units; indicated below). Almost all P-MARCKS was recovered in the cytosolic fraction.

stimulated phosphorylation by PKCε regulates the association of MARCKS with the membrane and/or the cytoskeleton.

### *MARCKS Silencing Abolishes Growth Cones*

MARCKS seems to exert its functional effects when bound to the plasma membrane, and phosphorylation by PKC inhibits this association. We sought to reduce MARCKS levels, and as a consequence membrane association, by silencing its expression. DRG neurons were cotransfected with MARCKS-targeted siRNA (siMARCKS) and a plasmid encoding GFP for identification. Transfection with siRNA targeted to nuclear lamin (siLamin), a functionally unrelated molecule, served as control. siLamin, which activated the RNA interference mechanism as indicated by reduced lamin immunolabeling of nuclear envelopes, did not change MARCKS levels or the morphology of growth cones (Supplemental Figure 2, top). Conversely, neurons transfected with siMARCKS exhibited normal nuclear lamin labeling (Supplemental Figure 2, bottom) but dramatically changed growth cones. Neurons transfected with siMARCKS initially formed apparently normally growing neurites. However, by 12 h in culture, transfected growth cones had decreased in size and often were reduced to fusiform structures that contained only sparse spots of MARCKS label (Figure 6, A and B). Untransfected neurons in the same cultures, however, exhibited the normal, broadly attached growth cone morphology typical of DRG neurons grown on laminin, with extensive MARCKS label (Figure 6G). At 18 h in culture (Figure 6, C–E), most neurites of siMARCKS neurons were largely devoid of detectable MARCKS. Strikingly, such neurites often ended as stubs (Figure 6C) or filamentous structures (Figure 6D). All neurites of transfected neurons exhibited a dramatic reduction in growth cone spread compared with control neurons transfected with GFP only. Growth cone area was measured in phase-contrast images as that covered by the distalmost linear 20 μm of the neurite/growth cone. As shown in Figure 7A, the reduction in area was greater than 10-fold and highly significant. Occasional neurons lacked neurites altogether (Figure 6E). At 24 h after transfection with siMARCKS, neurons (identified by GFP fluorescence and immunolabeling for the neuron-specific marker tubulin βIII) were devoid of neurites (Figure 6F). These results indicate that MARCKS is essential for the spread out, broadly adherent configuration of the growth cone and the long-term survival of the neurite.

### *Growth Cones Overexpressing MARCKS Are More Resistant to Phorbol Ester-induced Collapse*

Repellent action triggers adhesion complex disassembly via the 12(*S*)-HETE-PKCε pathway (Mikule *et al*., 2002). If MARCKS is indeed an effector of this pathway and a regulator of adhesion, then its overexpression should alter the growth cone's repellent response. To test this assertion, dissociated DRG neurons were transfected with a plasmid encoding wild-type MARCKS fused at its C terminus with GFP (wtMARCKS-GFP). The resulting fusion protein has been shown by others to dissociate from the membrane upon phosphorylation by activated PKC (Ohmori *et al*., 2000; Sawano *et al*., 2002; also see Myat *et al*., 1998). We challenged control and wtMARCKS-GFP–expressing growth cones with the PKC activator TPA to trigger collapse at the signaling step immediately preceding MARCKS phosphorylation and to elicit the strongest possible effect. When treated with TPA (Figure 8) nontransfected growth cones responded rapidly, with nearly complete collapse occurring within 5 min of TPA treatment (Figure 8, phase contrast, top row). To generate IRM image series of these rapid events was challenging. Nevertheless, Figure 8 (second row) shows that close contacts (IRM dark) rapidly decreased in total area in such growth cones and gave way to progressive detachment and retraction. In contrast, growth cones expressing wtMARCKS-GFP seemed remarkably stable under the same conditions (Figure 8, bottom). IRM images of such growth cones exhibited large areas of high density that shifted over time and sometimes included circular profiles of unknown nature. These may be attributed in part to changes in the surface topography of these very thinly spread growth cones and therefore must be interpreted with caution. However, the IRM images showed persistence of close contacts, for example, along the edges of the growth cone, and some of these could be seen to correlate with increased levels of wtMARCKS-GFP fluorescence. Collapse of transfected growth cones occurred very slowly, only after 15min of TPA exposure, in all wtMARCKS-GFP–overexpressing growth cones observed (n = 7). These growth cones also were moving very slowly or not at all so that they were not amenable to turning assay analysis.

### *Expression of Phosphorylation-deficient MARCKS Increases Growth Cone Adhesion*

If phosphorylation and translocation of MARCKS from membrane sites to the cytosol is a critical step in the regulation of attachment, then expression of phosphorylation-deficient mutant MARCKS should alter growth cone adhesion. To test this hypothesis, DRG neurons were transfected with a MARCKS mutant lacking the ED (MARCKS-ED), the site of PKC-dependent phosphorylation. We chose this mutant because expression of MARCKS-ED (or of the analogous mutant of macrophage MARCKS) had been shown to exert dominant-negative effects on microdomain formation and cell spreading (Li *et al*., 1996; Laux *et al*., 2000). For identification of transfected neurons, we coexpressed GFP by using a bicistronic vector.

MARCKS-ED–expressing growth cones retained the characteristic paddle shape seen in controls. However, they were much larger than control growth cones and exhibited more filopodia (compare Figures 3 and 9). These two parameters were analyzed quantitatively. Although control DRG growth cones on laminin formed on average only 1.5 ± 0.5 filopodia/growth cone (mean ± SEM; n = 10), their transfected counterparts had 13.8 ± 2.2 (n = 4, $p < 2 \times 10^{-6}$). Measurements of growth cone size are shown in Figure 7A. Relative to GFP controls, the average growth cone increased 1.7-fold in area upon MARCKS-ED transfection. The growth cone's aggregate close contact area, albeit a relatively small fraction (on average, 7.4% of the total area in GFP-only controls), increased even more, 2.2-fold (to an average 9.6% of total area; Figure 7B). These changes were highly significant. Expression of MARCKS-ED also altered the distributions of both MARCKS and $\alpha_3$-integrin within the growth cone's adhesive plane (Figure 9, A–C). The entire substrate contact area of the growth cone was covered by a reticular pattern of extensively overlapping MARCKS and $\alpha_3$-integrin label (MARCKS antibody recognized both wt and mutant forms). However, overlap was not complete (e.g., near asterisk in Figure 9C), indicating that this was not a "bleed-through" artifact. Colocalization was analyzed as for controls (see above), and the results are shown in Figure 4, B and C, and in Table 1. Both Manders' coefficients (R and $R_T$) were increased greatly and significantly relative to control throughout the growth cone but especially in the proximal area. As shown in Figure 4, B and C, >70% of PAZ integrin and MARCKS were colocalized, and in the proximal region the same values increased from ~20% in controls to 60%.

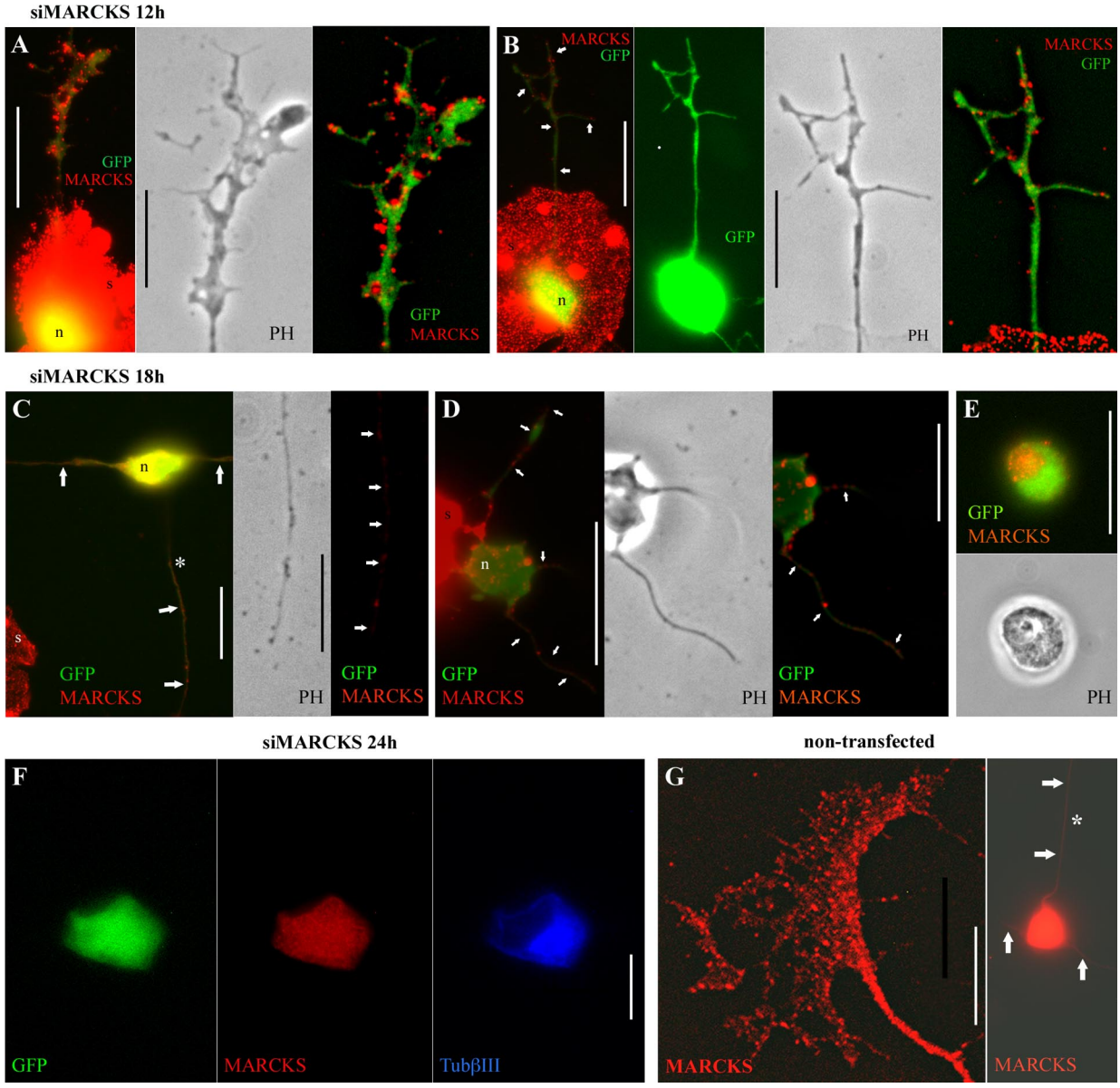


**Figure 6.** Silencing MARCKS expression in DRG neurons. All experiments included a GFP-encoding plasmid to identify transfected cells. Cells were immunostained for MARCKS (red). (A and B) siMARCKS, 12 h. Transfected neurons contain reduced but variable amounts of MARCKS, and the degree of growth cone spreading seems to correlate with MARCKS levels. The lower power micrographs (left; bar, 20 $\mu$m) show neuronal perikarya (n) sitting on top of supporting cells (s). The higher power pictures of growth cones (bar, 10 $\mu$m) are either phase contrast (PH) or merged, digitally deconvolved fluorescence images. (C–E) siMARCKS 18 h. Growth cones are not detectable but neurites can be observed. Left, neuronal perikarya and neurites (arrows) at lower power (bar, 20 $\mu$m). Phase contrast and deconvolved fluorescence images are shown at higher power to the right (bar, 10 $\mu$m). In C, asterisk marks the neurite shown at higher power. (E) Phase contrast and fluorescence micrographs showing a neuron without neurites. Immunofluorescence shows some MARCKS remnants. Bar, 20 $\mu$m. (F) siMARCKS, 24 h posttransfection. Neurons lack neurites. MARCKS immunofluorescence seems to recover, but it has not reached control level. Labeling with the marker tubulin $\beta$III identifies this cell as a neuron. (G) Growth cone and perikaryon (right) of a nontransfected neuron in a culture 12 h after transfection. The growth cone image (bar, 10 $\mu$m) shows MARCKS immunofluorescence after digital deconvolution. Fluorescence in this panel is reproduced so as to allow direct comparison with other growth cones in this figure. The image of the perikaryon was enhanced to show the neurites (arrows), especially the one (asterisk) that gave rise to the growth cone shown on the left.

Colocalization of most MARCKS with $\alpha_3$-integrin strongly suggested that overexpressed mutant MARCKS remained associated with the adherent plasmalemma. Indeed, the $\alpha_3$-integrin/MARCKS distribution was consistent with the reticular pattern of close adhesions, observed by IRM, that covered the entire growth cone area (Figure 9D; compare to GFP-only control, Figure 9E). As shown in Figure 9F, the actin cytoskeleton also was affected by MARCKS-ED expression. Instead of the radial F-actin pattern observed in all controls (Figure 9G; in 10 of 10 growth cones assessed), MARCKS-ED growth cones exhibited a criss-crossing meshwork of filaments highlighted by occasional knot-like structures (Figure 9F, arrows; present in all of 4 phalloidin-labeled samples). The knot-like F-actin aggregates were 0.50 $\pm$ 0.006 $\mu$m in diameter (mean $\pm$ SEM; n = 100) and abundant in all MARCKS-ED growth

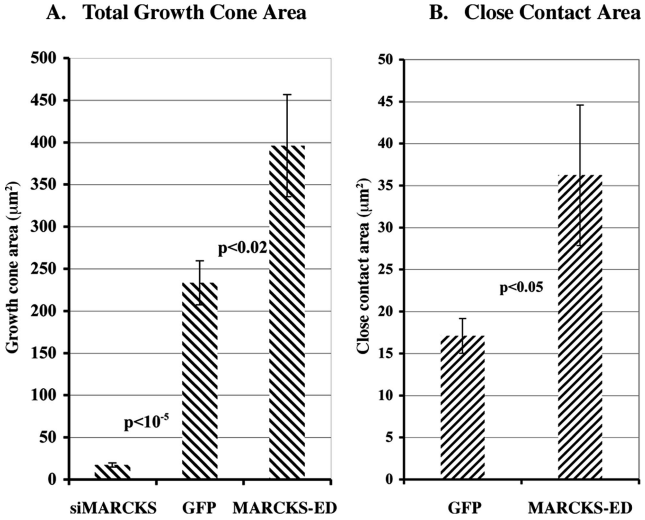


**Figure 7.** Effects of siMARCKS and MARCKS-ED expression on total growth cone area (A) and on aggregate close contact area (B). DRG neurons were transfected with GFP only, siMARCKS, or MARCKS-ED plus GFP, and they were grown on laminin. In siMARCKS neurons, growth cone areas were defined as those covered by the distal-most linear 20 $\mu$m of the neurite/growth cone and measured in phase-contrast images. For GFP only and MARCKS-ED plus GFP growth cones, IRM images were analyzed by thresholding to determine total and adhesive areas. Results are expressed as mean areas in square micrometers ± SEM. For GFP only, n = 20; for siMARCKS, n = 11; and for MARCKS-ED plus GFP, n = 22.

cones (159 ± 56/growth cone; mean ± SEM; n = 4). In contrast, similar aggregates were rare in controls (2.8 ± 1.0/growth cone; n = 10; $p < 0.0002$). It follows that MARCKS-ED expression qualitatively and quantitatively changed the growth cones' adhesive structures as seen by IRM, $\alpha_3$-integrin plus MARCKS distribution, and actin cytoskeleton configuration.

### *Growth Cones Expressing MARCKS-ED Lose Their Collapse Response to 12(S)-HETE and Their Turning Response to Sema3A*

The collapse response of growth cones to exogenous 12(*S*)-HETE was measured in neurons transfected with GFP only versus GFP plus MARCKS-ED, to determine whether MARCKS-ED conferred resistance to collapse induced by PKC$\varepsilon$ activation (Figure 10). Within 7.5 min after eicosanoid challenge growth cones expressing MARCKS-ED did not respond to exogenous 12(*S*)-HETE, whereas control growth cones did. The 12(*S*)-HETE-induced reduction in area of GFP-expressing control growth cones (~20%) was almost identical to that of nontransfected DRG growth cones of explant cultures under similar experimental conditions (Mikule *et al*., 2002). In MARCKS-ED transfectants, however, the response was reduced to 4 ± 5% ($p < 0.05$).

The data presented thus far are consistent with nonphosphorylated MARCKS acting to promote growth cone adhesion and thereby to inhibit collapse. Is MARCKS phosphorylation required for accurate growth cone pathfinding? To

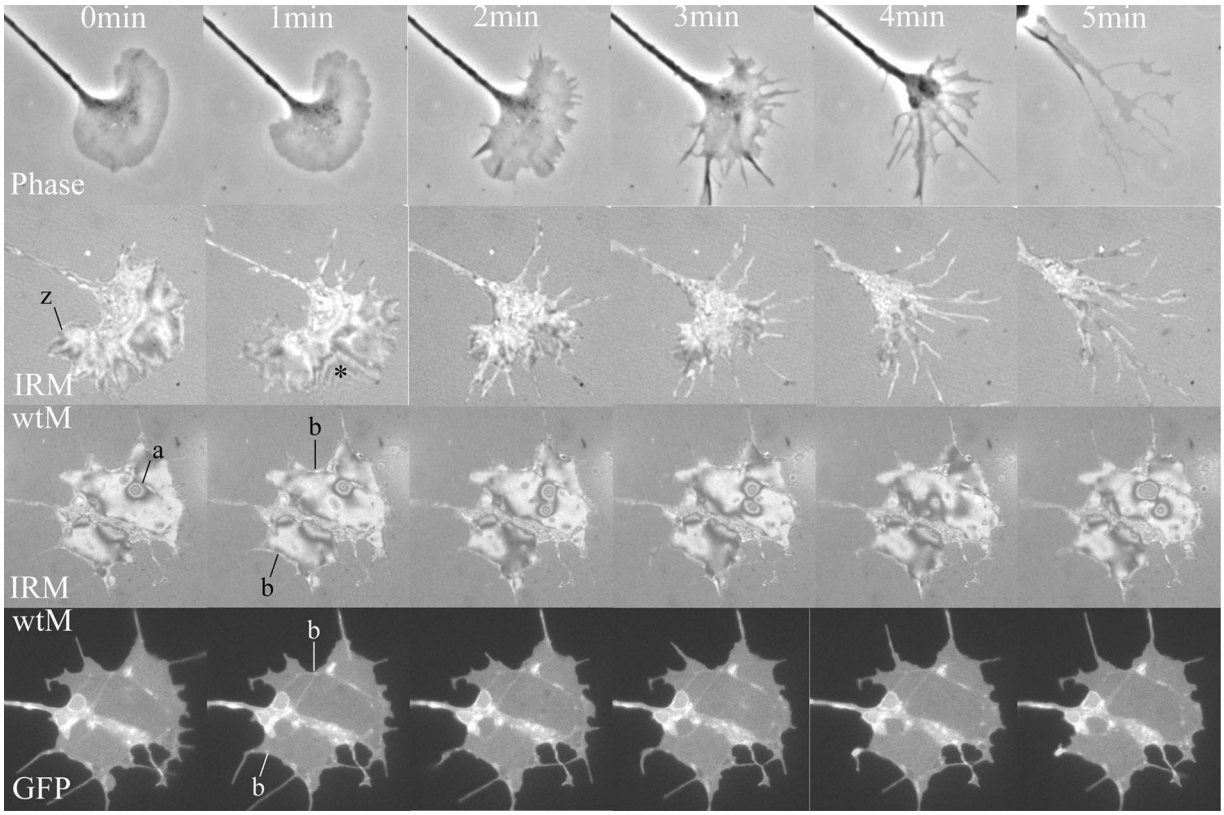


**Figure 8.** Effect of wtMARCKS-GFP overexpression on TPA-stimulated growth cone collapse. Growth cones of DRG neurons were challenged with 1 $\mu$M TPA (0 min, onset of TPA treatment). Top row, time series (taken at 1-min intervals) of phase-contrast images of a nontransfected growth cone. Second row, time series of IRM images of a different, nontransfected growth cone. z, PAZ; asterisk, area of higher order interference. Third and fourth rows, IRM and fluorescence images of a DRG growth cone expressing wtMARCKS-GFP. a, circular profile of unknown nature, possibly owing to the thinned out growth cone's surface topography; b, regions where close contacts coincide with concentrations of wtMARCKS-GFP fluorescence. Growth cones are shown at the same scale.

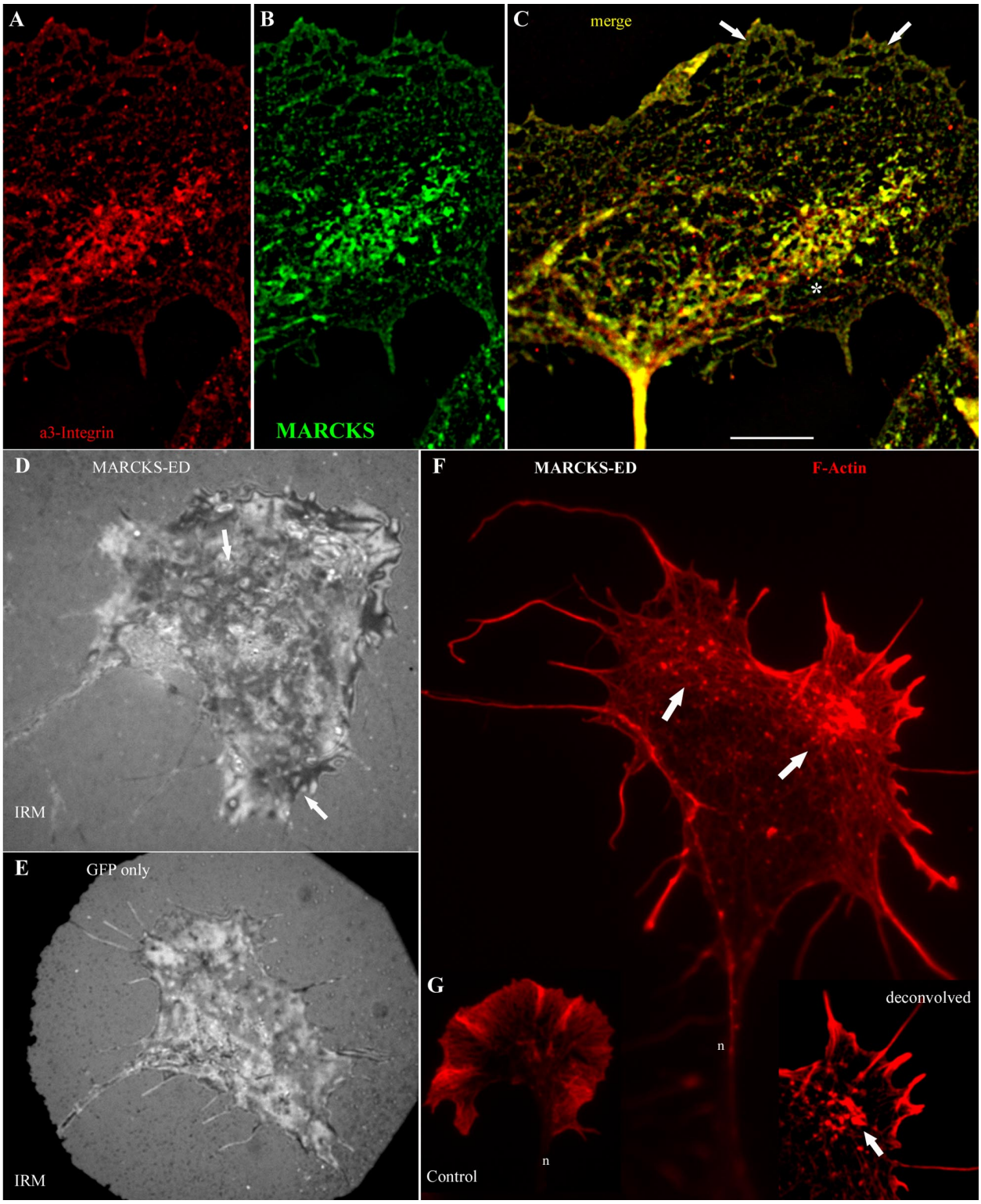


**Figure 9.** Effect of MARCKS-ED expression on growth cone adhesion and the actin cytoskeleton. (A and B) Single-channel immunofluorescence micrographs of a growth cone growing on laminin and expressing MARCKS-ED, as identified by GFP fluorescence (not shown). Anti-$\alpha_3$-integrin (Alexa Fluor 647-conjugated secondary antibody), rendered in red pseudocolor (A); anti-MARCKS (Alexa Fluor 594-conjugated secondary antibody), rendered in green pseudocolor (B). (C) Merged image. Although overlap (yellow) is extensive, it is not complete, as shown, e.g., in the area marked by asterisk. (D and E) IRM images of growth cones expressing MARCKS-ED and GFP alone, respectively. The arrows in C and D point at reticular pattern of integrin and MARCKS label (C) and of IRM-dense adhesions (D) in MARCKS-ED–expressing growth cones. (F and G) Texas Red-phalloidin labeling of a MARCKS-ED–expressing and control growth cone, respectively. The arrows point at abnormal F-actin distribution, also shown in the inset (deconvolved image). n, neurites. Note large size of MARCKS-ED growth cones relative to controls (see Figure 3). All growth cones are shown at the same magnification (bar, 10 $\mu$m).

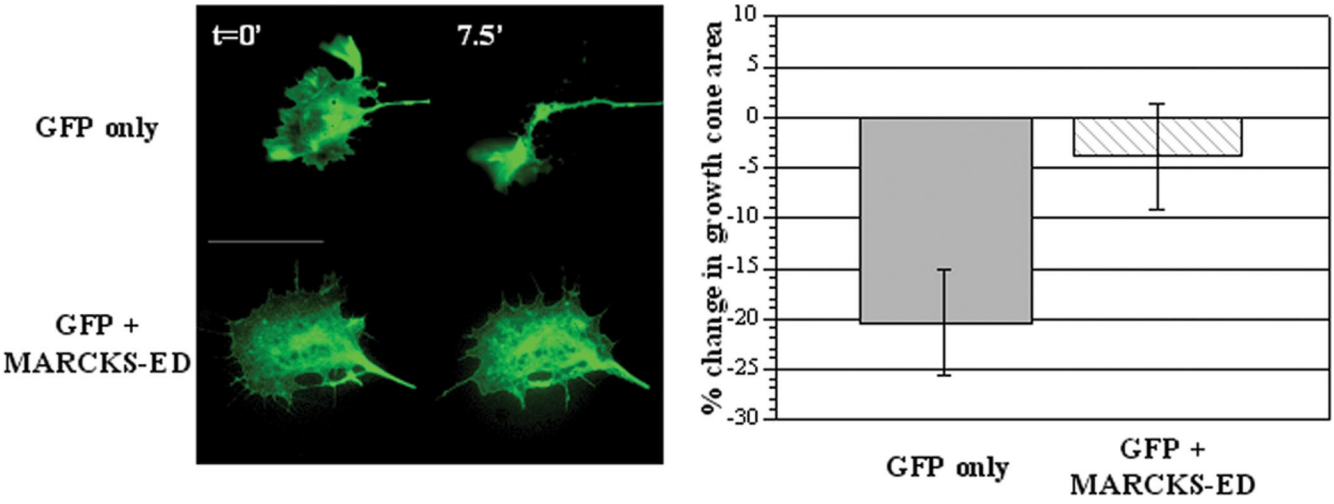


**Figure 10.** Effect of MARCKS-ED expression on 12(*S*)-HETE-induced growth cone collapse. Fluorescence micrographs of growth cones expressing GFP alone (left, top row), or GFP and MARCKS-ED (left, bottom row). Images were taken just before (t = 0 min) or 7.5 min after $10^{-8}$ M 12(*S*)-HETE addition to the culture medium. Graph on right shows quantitative analysis of collapse. Growth cone areas were measured at t = 0 min and at 7.5 min after treatment. Results are expressed as mean change in growth cone area ± SEM. For GFP only, n = 13; and for MARCKS-ED plus GFP, n = 11.

address this question, we used turning assays to measure the response of growth cones to microgradients of Sema3A. MARCKS-ED-expressing DRG growth cones were compared with controls, which expressed GFP only. Control growth cones (from dissociated neurons) responded to Sema3A gradients just like nontransfected growth cones (from neurons in explant cultures; compare Figures 2 and 11), with a final turning angle of 13.5 ± 4° away from the repellent source. Thus, GFP expression alone or the cell dissociation required for neuron transfection did not affect the growth cones' turning response. However, expression of MARCKS-ED significantly altered growth cone turning in Sema3A gradients. Not only did MARCKS-ED abrogate Sema3A-induced repulsion but also it caused the majority of growth cones to turn toward the repellent source (Figure 11A, right). The difference between average final turning angles for growth cones of MARCKS-ED neurons versus those of GFP-only neurons was highly significant ($p < 0.005$). An additional comparison of interest was with the response of nontransfected growth cones to control medium (Figure 2, B and C). In these controls, growth cones were neither attracted to, nor repulsed from, the micropipette tip

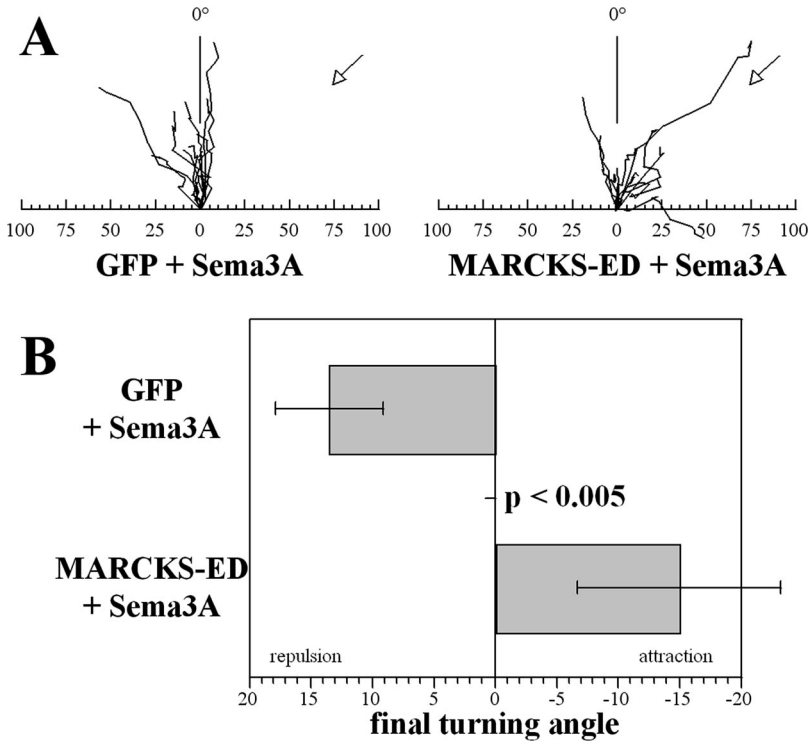


**Figure 11.** Effect of MARCKS-ED expression on Sema3A-mediated growth cone repulsion. Growth cone turning experiments were performed as described in Figure 2. (A) Rosebud plots depicting 1-h traces of growth cones exposed to Sema3A gradients. Growth cones were expressing either GFP only (left), or GFP and MARCKS-ED (right). B, average final turning angles, calculated as in Figure 2 (means ± SEM). Value for the extreme neurite dipping below the abscissa (right) was excluded from the statistical analysis. For GFP only, n = 12; for MARCKS-ED plus GFP, n = 11).

(final turning angle of 1 ± 3°). The MARCKS-ED growth cones exposed to Sema3A gradients, however, moved toward the micropipette tip and generated final turning angles (−15 ± 8°) that were significantly different ($p < 0.05$) from those of controls. This indicated that MARCKS-ED expression switched Sema3A-induced repulsion to attraction.

## DISCUSSION

### *PKC Activity Is Required for Sema3A-induced Growth Cone Turning*

Growth cone challenge by phorbol ester triggers rapid collapse if globally applied (Fournier *et al.*, 2000) or chemorepulsion if applied as a gradient (Xiang *et al.*, 2002). These results demonstrate that PKC activity is sufficient for growth cone turning and collapse, but they provide no evidence that PKC is an effector in repellent-initiated signaling cascades. Our laboratory demonstrated that Sema3A-induced growth cone collapse requires the synthesis of 12(*S*)-HETE (Mikule *et al.*, 2002), that this eicosanoid directly and selectively activates PKCε (Mikule *et al.*, 2003), and that Sema3A requires PKC activity for collapse induction. Similarly, a novel (i.e., $Ca^{2+}$-independent) PKC activity is required for EphrinA5-mediated growth cone collapse (Wong *et al.*, 2004). Our new observation that growth cones fail to respond to microgradients of Sema3A in the presence of the PKC inhibitor Bis demonstrates that the more complex growth cone response of turning also requires PKC activity.

### *The PKC Substrate MARCKS Is a Component of Growth Cone Adhesions*

The only molecular constituents common to all known cell–matrix adhesions are the integrins, a family of membrane-spanning, heterodimeric receptors for matrix ligands (for review, see Hynes, 1992). DRG growth cones are known to express three types of laminin-binding integrins, including $\alpha_3\beta_1$ (McKerracher *et al.*, 1996). The distribution of $\alpha_3$-integrin in the laminin-attached plasma membrane of DRG growth cones (permeabilized in mild conditions) was consistent with that of close contacts, especially those in the PAZ. MARCKS immunoreactivity exhibited a similar pattern, and it was the PAZ where MARCKS and $\alpha_3$-integrin showed the greatest amount of colocalization.

We previously showed that MARCKS forms a punctate pattern in the adhesive plasmalemma of DRG growth cones (Mikule *et al.*, 2003), just as reported for other putative adhesion proteins (Arregui *et al.*, 1994; Renaudin *et al.*, 1999), but there was little or no overlap with the adhesion site proteins, talin, vinculin, paxillin, or focal adhesion kinase, and none of the latter exhibited distributions that spatially correlated with the PAZ (Arregui *et al.*, 1994; Mikule *et al.*, 2003). However, these data were obtained under harsher (Triton X-100) permeabilization conditions than those used here (Brij 98). The present results demonstrate for the first time in growth cones a clear correlation between adhesion as observed by IRM and immunolocalization of the adhesion site protein $\alpha_3$-integrin colocalized with MARCKS. This colocalization and spatial correlation identify MARCKS as a component of functional adhesion sites within the growth cone.

### *MARCKS Regulates Axonal Guidance by Stabilizing Growth Cone Adhesions*

If the phosphorylation and dissociation of MARCKS from growth cone plasmalemma is required for repellent action and growth cone detachment, then overexpression of wt-MARCKS or of the nonphosphorylatable MARCKS-ED mutant would be expected to provoke an aberrant repellent response characterized by defective de-adhesion. Indeed, growth cones overexpressing wtMARCKS-GFP exhibited a much slower collapse response to TPA than nontransfected controls. This was unlikely to be the result of MARCKS fusion with GFP because wtMARCKS-GFP is known to cycle normally between the plasma membrane and the cytosol (Ohmori *et al.*, 2000; Sawano *et al.*, 2002). In contrast to wtMARCKS overexpression, MARCKS knockdown resulted in neurites whose growth cones' substrate adhesion decreased with diminishing MARCKS levels until they ended as stubs without terminal enlargement. At this point, neurites disappeared, probably by detachment and retraction.

Growth cones expressing MARCKS-ED exhibited a greatly increased, extensive network of close adhesions seen by IRM and characterized by greatly enhanced $\alpha_3$–integrin–MARCKS colocalization. They were essentially unresponsive to the detaching/collapsing agent 12(*S*)-HETE and were not repulsed by gradients of Sema3A. Deletion of the ED removed not only the PKC phosphorylation sites but also the basic amino acids involved in membrane binding. However, MARCKS-ED was extensively associated with the adhesive plasmalemma of the growth cone, and the adhesive area was greatly expanded. Thus, MARCKS-ED must interact selectively with membrane components of growth cone adhesions via domain(s) other than the ED (Swierczynski and Blackshear, 1995; Seykora *et al.*, 1996; Laux *et al.*, 2000). Because growth cone collapse and turning require release of adhesions, MARCKS-ED inhibition of repulsion and detachment establishes a role for wtMARCKS as stabilizer of adhesions. The observation that MARCKS-ED expression switched Sema3A-induced repulsion to attraction is more difficult to explain, and we do not fully understand the nature or mechanism of this repulsion–attraction switch. A possible explanation would be that growth cones expressing MARCKS-ED also contained wtMARCKS protein and that both participated initially in growth cone adhesion. Thus, Sema3A in the gradient could still cause detachment of growth cone adhesions containing wtMARCKS and allow subsequent spreading. However, the new adhesions would contain progressively more MARCKS-ED, locking them against the substratum. This would, at least for a limited period, cause the growth cone to move toward the repellent source. Regardless, our results strikingly emphasize 1) MARCKS' role as a stabilizer of adhesion and 2) the role of adhesion control in growth cone steering.

Although many reports indicate MARCKS' involvement in adhesion mechanisms, a clear picture of how MARCKS functions has yet to emerge. Cells expressing constitutively membrane-associated MARCKS mutants exhibit deficient spreading and adhesion (Swierczynski and Blackshear, 1995; Myat *et al.*, 1997; Spizz and Blackshear, 2001), as analyzed at the initial stages of cell spreading. In contrast, studies on MARCKS function in spread, well-anchored cells suggested that the protein enhanced cell–matrix adhesion (Manenti *et al.*, 1997; Iioka *et al.*, 2004), consistent with our observations in growth cones (also see Calabrese and Halpain, 2005). How MARCKS can function to both inhibit cell spreading yet increase adhesion in cells already broadly attached remains to be determined. One possibility is that MARCKS is involved in stabilizing integrins (ligand-engaged or not) in their high-affinity state and in limiting their lateral movement in the membrane, thus enhancing adhesion once established; yet, the formation of new adhesions, which requires integrin mobility (Li *et al.*, 1996), would be inhibited by MARCKS.

## CONCLUSIONS

Together with our previous results, the data presented here demonstrate that 12(*S*)-HETE-stimulated PKCε activity is necessary for Sema3A-induced repulsion and identify its substrate, MARCKS, as a regulatory component of growth cone adhesion complexes. These results are consistent with the concept that repellent-induced 12(*S*)-HETE stimulation of MARCKS phosphorylation causes growth cone detachment. Expression of a phosphorylation-deficient MARCKS mutant did indeed increase growth cone adhesion, lead to extensive integrin–MARCKS colocalization, and render growth cones refractory to 12(*S*)-HETE–induced collapse and Sema3A-mediated repulsion. Conversely, silencing MARCKS expression caused reduction of attached growth cone area. These results indicate that nonphosphorylated MARCKS acts as a stabilizer of growth cone adhesion via interaction with adhesion site proteins. Therefore, we propose a model for the regulation of growth cone adhesion in which phosphorylation by PKCε releases MARCKS from adhesion sites, resulting in their destabilization, growth cone detachment, and turning or collapse. That phosphorylation-deficient MARCKS and the ensuing deficit in adhesion control convert Sema3A-induced repulsion into attraction highlights the importance of adhesion control in growth cone pathfinding.

## ACKNOWLEDGMENTS

We thank Drs. Kristin Schaller and Greg Bird (School of Medicine, University of Colorado) for generous help with MARCKS vector construction. This work was supported by National Institutes of Health (NIH) Grant R01 NS41029 (to K.H.P., principal investigator), NIH National Research Service Award (NRSA) F31 NS44705 (to J.C.G.), and NIH NRSA F31 NS48710 (to S.D.S.).

## REFERENCES

Aizawa, H., *et al*. (2001). Phosphorylation of cofilin by LIM-kinase is necessary for semaphorin 3A-induced growth cone collapse. Nat. Neurosci. *4*, 367–373.

Allen, L. A., and Aderem, A. (1995). Protein kinase C regulates MARCKS cycling between the plasma membrane and lysosomes in fibroblasts. EMBO J. *14*, 1109–1120.

Arregui, C. O., Carbonetto, S., and McKerracher, L. (1994). Characterization of neural cell adhesion sites: point contacts are the sites of interaction between integrins and the cytoskeleton in PC12 cells. J. Neurosci. *14*, 6967–6977.

Barberis, D., Artigiani, S., Casazza, A., Corso, S., Giordano, S., Love, C. A., Jones, E. Y., Comoglio, P. M., and Tamagnone, L. (2004). Plexin signaling hampers integrin-based adhesion, leading to Rho-kinase independent cell rounding, and inhibiting lamellipodia extension and cell motility. FASEB J. *18*, 592–594.

Berditchevski, F., and Odintsova, E. (1999). Characterization of integrin-tetraspanin adhesion complexes: role of tetraspanins in integrin signaling. J. Cell Biol. *146*, 477–492.

Blackshear, P. J., Silver, J., Nairn, A. C., Sulik, K. K., Squier, M. V., Stumpo, D. J., and Tuttle, J. S. (1997). Widespread neuronal ectopia associated with secondary defects in cerebrocortical chondroitin sulfate proteoglycans and basal lamina in MARCKS-deficient mice. Exp. Neurol. *145*, 46–61.

Bubb, M. R., Lenox, R. H., and Edison, A. S. (1999). Phosphorylation-dependent conformational changes induce a switch in the actin-binding function of MARCKS. J. Biol. Chem. *274*, 36472–36478.

Calabrese, B., and Halpain, S. (2005). Essential role for the PKC target MARCKS in maintaining dendritic spine morphology. Neuron *48*, 77–90.

Costes, S. V., Daelemans, D., Cho, E. H., Dobbin, Z., Pavlakis, G., and Lockett, S. (2004). Automatic and quantitative measurement of protein-protein colocalization in live cells. Biophys. J. *86*, 3993–4003.

Cypher, C., and Letourneau, P. C. (1991). Identification of cytoskeletal, focal adhesion, and cell adhesion proteins in growth cone particles isolated from developing chick brain. J. Neurosci. Res. *30*, 259–265.

de la Houssaye, B. A., Mikule, K., Nikolic, D., and Pfenninger, K. H. (1999). Thrombin-induced growth cone collapse: involvement of phospholipase A(2) and eicosanoid generation. J. Neurosci. *19*, 10843–10855.

Disatnik, M. H., Boutet, S. C., Lee, C. H., Mochly-Rosen, D., and Rando, T. A. (2002). Sequential activation of individual PKC isozymes in integrin-mediated muscle cell spreading: a role for MARCKS in an integrin signaling pathway. J. Cell Sci. *115*, 2151–2163.

Disatnik, M. H., Boutet, S. C., Pacio, W., Chan, A. Y., Ross, L. B., Lee, C. H., and Rando, T. A. (2004). The bi-directional translocation of MARCKS between membrane and cytosol regulates integrin-mediated muscle cell spreading. J. Cell Sci. *117*, 4469–4479.

Fan, J., and Raper, J. A. (1995). Localized collapsing cues can steer growth cones without inducing their full collapse. Neuron *14*, 263–274.

Fournier, A. E., Kalb, R. G., and Strittmatter, S. M. (2000). Rho GTPases and axonal growth cone collapse. Methods Enzymol. *325*, 473–482.

Gundersen, R. W. (1988). Interference reflection microscopic study of dorsal root growth cones on different substrates: assessment of growth cone-substrate contacts. J. Neurosci. Res. *21*, 298–306.

Gungabissoon, R. A., and Bamburg, J. R. (2003). Regulation of growth cone actin dynamics by ADF/cofilin. J. Histochem. Cytochem. *51*, 411–420.

Hartwig, J. H., Thelen, M., Rosen, A., Janmey, P. A., Nairn, A. C., and Aderem, A. (1992). MARCKS is an actin filament crosslinking protein regulated by protein kinase C and calcium-calmodulin. Nature *356*, 618–622.

Huber, A. B., Kolodkin, A. L., Ginty, D. D., and Cloutier, J. F. (2003). Signaling at the growth cone: ligand-receptor complexes and the control of axon growth and guidance. Annu. Rev. Neurosci. *26*, 509–563.

Hynes, R. O. (1992). Integrins: versatility, modulation, and signaling in cell adhesion. Cell *69*, 11–25.

Iioka, H., Ueno, N., and Kinoshita, N. (2004). Essential role of MARCKS in cortical actin dynamics during gastrulation movements. J. Cell Biol. *164*, 169–174.

Izzard, C. S., and Lochner, L. R. (1976). Cell-to-substrate contacts in living fibroblasts: an interference reflexion study with an evaluation of the technique. J. Cell Sci. *21*, 129–159.

Jin, Z., and Strittmatter, S. M. (1997). Rac1 mediates collapsin-1-induced growth cone collapse. J. Neurosci. *17*, 6256–6263.

Jockusch, B. M., Bubeck, P., Giehl, K., Kroemker, M., Moschner, J., Rothkegel, M., Rudiger, M., Schluter, K., Stanke, G., and Winkler, J. (1995). The molecular architecture of focal adhesions. Annu. Rev. Cell Dev. Biol. *11*, 379–416.

Katz, F., Ellis, L., and Pfenninger, K. H. (1985). Nerve growth cones isolated from fetal rat brain. III. Calcium-dependent protein phosphorylation. J. Neurosci. *5*, 1402–1411.

Kim, J., Blackshear, P. J., Johnson, J. D., and McLaughlin, S. (1994). Phosphorylation reverses the membrane association of peptides that correspond to the basic domains of MARCKS and neuromodulin. Biophys. J. *67*, 227–237.

Laux, T., Fukami, K., Thelen, M., Golub, T., Frey, D., and Caroni, P. (2000). GAP43, MARCKS, and CAP23 modulate PI(4,5)P(2) at plasmalemmal rafts, and regulate cell cortex actin dynamics through a common mechanism. J. Cell Biol. *149*, 1455–1472.

Lee, J., and Jacobson, K. (1997). The composition and dynamics of cell-substratum adhesions in locomoting fish keratocytes. J. Cell Sci. *110*, 2833–2844.

Letourneau, P. C., and Shattuck, T. A. (1989). Distribution and possible interactions of actin-associated proteins and cell adhesion molecules of nerve growth cones. Development *105*, 505–519.

Li, J., Zhu, Z., and Bao, Z. (1996). Role of MacMARCKS in integrin-dependent macrophage spreading and tyrosine phosphorylation of paxillin. J. Biol. Chem. *271*, 12985–12990.

Lohof, A. M., Quillan, M., Dan, Y., and Poo, M. M. (1992). Asymmetric modulation of cytosolic cAMP activity induces growth cone turning. J. Neurosci. *12*, 1253–1261.

Lohse, K., Helmke, S. M., Wood, M. R., Quiroga, S., de la Houssaye, B. A., Miller, V. E., Negre-Aminou, P., and Pfenninger, K. H. (1996). Axonal origin and purity of growth cones isolated from fetal rat brain. Brain Res. Dev. Brain Res. *96*, 83–96.

Manenti, S., Malecaze, F., and Darbon, J. M. (1997). The major myristoylated PKC substrate (MARCKS) is involved in cell spreading, tyrosine phosphorylation of paxillin, and focal contact formation. FEBS Lett. *419*, 95–98.

McKerracher, L., Chamoux, M., and Arregui, C. O. (1996). Role of laminin and integrin interactions in growth cone guidance. Mol. Neurobiol. *12*, 95–116.

McLaughlin, S., and Aderem, A. (1995). The myristoyl-electrostatic switch: a modulator of reversible protein-membrane interactions. Trends Biochem. Sci. *20*, 272–276.

Messersmith, E. K., Leonardo, E. D., Shatz, C. J., Tessier-Lavigne, M., Goodman, C. S., and Kolodkin, A. L. (1995). Semaphorin III can function as a selective chemorepellent to pattern sensory projections in the spinal cord. Neuron *14*, 949–959.

Mikule, K., Gatlin, J. C., de la Houssaye, B. A., and Pfenninger, K. H. (2002). Growth cone collapse induced by semaphorin 3A requires 12/15-lipoxygenase. J. Neurosci. *22*, 4932–4941.

Mikule, K., Sunpaweravong, S., Gatlin, J. C., and Pfenninger, K. H. (2003). Eicosanoid activation of protein kinase C epsilon: involvement in growth cone repellent signaling. J. Biol. Chem. *278*, 21168–21177.

Myat, M. M., Anderson, S., Allen, L. A., and Aderem, A. (1997). MARCKS regulates membrane ruffling and cell spreading. Curr. Biol. *7*, 611–614.

Myat, M. M., Chang, S., Rodriguez-Boulan, E., and Aderem, A. (1998). Identification of the basolateral targeting determinant of a peripheral membrane protein, MacMARCKS, in polarized cells. Curr. Biol. *8*, 677–683.

Ohmori, S., Sakai, N., Shirai, Y., Yamamoto, H., Miyamoto, E., Shimizu, N., and Saito, N. (2000). Importance of protein kinase C targeting for the phosphorylation of its substrate, myristoylated alanine-rich C-kinase substrate. J. Biol. Chem. *275*, 26449–26457.

Pfenninger, K. H., Ellis, L., Johnson, M. P., Friedman, L. B., and Somlo, S. (1983). Nerve growth cones isolated from fetal rat brain: subcellular fractionation and characterization. Cell *35*, 573–584.

Pfenninger, K. H., and Maylie-Pfenninger, M. F. (1981). Lectin labeling of sprouting neurons. I. Regional distribution of surface glycoconjugates. J. Cell Biol. *89*, 536–546.

Renaudin, A., Lehmann, M., Girault, J., and McKerracher, L. (1999). Organization of point contacts in neuronal growth cones. J. Neurosci. Res. *55*, 458–471.

Rosen, A., Keenan, K. F., Thelen, M., Nairn, A. C., and Aderem, A. (1990). Activation of protein kinase C results in the displacement of its myristoylated, alanine-rich substrate from punctate structures in macrophage filopodia. J. Exp. Med. *172*, 1211–1215.

Sawano, A., Hama, H., Saito, N., and Miyawaki, A. (2002). Multicolor imaging of Ca(2+) and protein kinase C signals using novel epifluorescence microscopy. Biophys. J. *82*, 1076–1085.

Schmidt, C. E., Dai, J., Lauffenburger, D. A., Sheetz, M. P., and Horwitz, A. F. (1995). Integrin-cytoskeletal interactions in neuronal growth cones. J. Neurosci. *15*, 3400–3407.

Seykora, J. T., Myat, M. M., Allen, L. A., Ravetch, J. V., and Aderem, A. (1996). Molecular determinants of the myristoyl-electrostatic switch of MARCKS. J. Biol. Chem. *271*, 18797–18802.

Spizz, G., and Blackshear, P. J. (2001). Overexpression of the myristoylated alanine-rich C-kinase substrate inhibits cell adhesion to extracellular matrix components. J. Biol. Chem. *276*, 32264–32273.

Suter, D. M., and Forscher, P. (2000). Substrate-cytoskeletal coupling as a mechanism for the regulation of growth cone motility and guidance. J. Neurobiol. *44*, 97–113.

Stumpo, D. J., Bock, C. B., Tuttle, J. S., and Blackshear, P. J. (1995). MARCKS deficiency in mice leads to abnormal brain development and perinatal death Proc. Natl. Acad. Sci. USA *92*, 944–948.

Swierczynski, S. L., and Blackshear, P. J. (1995). Membrane association of the myristoylated alanine-rich C kinase substrate (MARCKS) protein. Mutational analysis provides evidence for complex interactions. J. Biol. Chem. *270*, 13436–13445.

Thelen, M., Rosen, A., Nairn, A. C., and Aderem, A. (1991). Regulation by phosphorylation of reversible association of a myristoylated protein kinase C substrate with the plasma membrane. Nature *351*, 320–322.

Toullec, D., *et al*. (1991). The bisindolylmaleimide GF 109203X is a potent and selective inhibitor of protein kinase C. J. Biol. Chem. *266*, 15771–15781.

Towbin, H., Staehelin, T., and Gordon, J. (1979). Electrophoretic transfer of proteins from polyacrylamide gels to nitrocellulose sheets: procedure and some applications. Proc. Natl. Acad. Sci. USA *76*, 4350–4354.

Wang, X. X., and Pfenninger, K. H. (2006). Functional analysis of SIRPalpha in the growth cone. J. Cell Sci. *119*, 172–183.

Wong, E. V., Kerner, J. A., and Jay, D. G. (2004). Convergent and divergent signaling mechanisms of growth cone collapse by ephrinA5 and slit2. J. Neurobiol. *59*, 66–81.

Xiang, Y., Li, Y., Zhang, Z., Cui, K., Wang, S., Yuan, X. B., Wu, C. P., Poo, M. M., and Duan, S. (2002). Nerve growth cone guidance mediated by G protein-coupled receptors. Nat. Neurosci. *5*, 843–848.